Quantum Process Tomography of Multichromophoric Systems via Ultrafast Spectroscopy

Quantum Process Tomography of Multichromophoric Systems via Ultrafast Spectroscopy

Joel Yuen-Zhou, Masoud Mohseni and Alán Aspuru-Guzik*

Department of Chemistry and Chemical Biology,

Harvard University, Cambridge, MA 02138

Abstract

The description of excited state dynamics in multichromophoric systems constitutes both a theoretical and experimental challenge in modern physical chemistry. An experimental protocol which can systematically characterize both coherent and dissipative processes at the level of the evolving quantum state of the chromophores is desired. In this article, we show that a carefully chosen set of polarization controlled two-color heterodyned photon-echo experiments can be used to reconstruct the time-evolving density matrix of the one-exciton manifold of a heterodimer. This possibility in turn allows for a complete description of the excited state dynamics via quantum process tomography (QPT). Calculations on the dimer show that QPT can reveal rich information about system-bath interactions, which otherwise appear nontrivially hidden in the polarization monitored in standard four-wave mixing experiments. Our study presents a novel method for analyzing condensed phase experiments with a quantum information processing perspective.

*Electronic address: aspuru@chemistry.harvard.edu

Multichromophoric systems in condensed phases and the processes triggered upon their interaction with electromagnetic radiation are of fundamental chemical interest [1–3]. In multidimensional optical spectroscopy, a series of ultrafast pulses induce coherent vibrational and electronic dynamics on a molecular aggregate, and the nonlinear polarization effected on the latter is monitored both in time and frequency domain [4, 5]. Recently, a series of *tour-de-force* spectroscopic experiments performed in the groups of Fleming, Scholes, and Engel [6–8] have presented intriguing evidence that electronic coherences prepared in photosynthetic complexes persist for hundreds of femtoseconds, contesting the popular belief that no quantum effects exist in "hot and wet" environments, and simultaneously fueling intense work on the theoretical side to understand the role of quantum coherence and entanglement in these biological systems [9–14]. To interpret these observations, theoretical modeling has proven to be essential, with the latter being intuitively formulated in the Liouville space formalism by Mukamel [15]. In that theory, the induced polarization is calculated as a convolution of a nonlinear response function with the pulse envelopes of the perturbations. Implicit in these calculations is the evolution of the quantum state of the dissipative system in consideration in the form of a density matrix. Therefore, the detected polarization contains information of the time dependent density matrix of the system, although admittedly, not in the most transparent way. An important problem arises whether quantum state tomography (QST) can be carried out in these experiments, that is, whether the density matrix can actually be imaged at different instants of time (for an example, see [16], which reports a QST experiment in gas phase molecules, or [17] which shows how to carry out QST for molecular wavepackets via nonlinear interferometry). A more ambitious question is whether a complete characterization of the relevant quantum system can be performed by quantum process tomography (QPT) [18], a protocol which we define below. In this article, we show that both QST and QPT possible, at least for the single-exciton manifold of a heterodimer of chromophores.

We begin by reviewing the basic ideas of QPT. Let S be a system of interest which interacts with a bath B, and suppose they are initially uncorrelated from one another, that is, $\rho_{SB}(0) = \rho_S(0) \otimes \rho_B(0)$, where $\rho_{SB}(T)$ denotes the total S and B density matrix at time T, and $\rho_S(T)$ and $\rho_B(T)$ indicate the corresponding reduced density matrices for S and B. We label the time argument with T, instead of the standard t, because our QPT is performed for each "waiting" time T in the photon-echo timeline (see Fig. 2). Assuming that S and B as a whole evolve unitarily via a total Hamiltonian H_{total}, and that the initial state of B is fixed at $\rho_B(0)$ for every $\rho_S(0)$, a trace over the degrees of freedom of B yields a completely positive map for $\rho_S(T)$ [19]:

$$\rho_{S,ab}(T) = \sum_{cd} \chi_{abcd}(T)\rho_{S,cd}(0), \tag{1}$$

where the $\chi(T)$ matrix defines a linear transformation independent of the initial state $\rho_S(0)$. Therefore, $\chi(T)$ completely characterizes the dynamics of $\rho_S(T)$, and has a simple interpretation: $\chi_{abcd}(T)$ is the entry $\rho_{S,ab}(T)$ of the density matrix of S at time T given that $\rho_{S,cd}(0)$ has been prepared as the initial state. Important symmetries of this transformation are,

$$\begin{aligned} \chi_{abcd}(T) &= \chi^*_{badc}(T) \\ \sum_a \chi_{aacd}(T) &= \delta_{cd}, \end{aligned} \tag{2}$$

which preserve the hermiticity and trace of $\rho_S(T)$, respectively. Operationally, QPT can be defined as the experimental protocol to obtain $\chi(T)$. Spectroscopically, $\chi(T)$ may be reconstructed by repeteadly preparing a complete set of initial states, waiting for evolution for time T, and finally measuring the resulting state in a complete basis [18, 20]. QPT has been experimentally implemented in a wide variety of scenarios, including nuclear magnetic resonance [21], ion traps [22], single photons [23, 24], solid state qubits [25], and optical lattices [26]. In this article, we show how to perform QPT for a model coupled heterodimer using two-color polarization controlled heterodyne photon-echo experiments.

The model system we shall study in this article is an excitonic system described by the Hamiltonian[5, 27, 28]:

$$H_S = \omega_A a_A^+ a_A + \omega_B a_B^+ a_B + J(a_A^+ a_B + a_B^+ a_A), \tag{3}$$

where a_i^+ and a_i are creation and anhilation operators for single excitons in the site $i \in \{A, B\}$, $\omega_A \neq \omega_B$ are the first and second site energies, and $J \neq 0$ is the Coulombic coupling between the chromophores. Equation (3) can be easily diagonalized in the single-exciton manifold to yield:

$$H_S = \omega_\alpha c_\alpha^+ c_\alpha + \omega_\beta c_\beta^+ c_\beta. \tag{4}$$

Here, c_j^+ and c_j are delocalized exciton operators labeled with $j \in \{\alpha, \beta\}$. We label these one-exciton states as $|\alpha\rangle = c_\alpha^+|g\rangle$, $|\beta\rangle = c_\beta^+|g\rangle$, where $|g\rangle$ is the excitonic vaccuum. We also consider the biexcitonic state $|f\rangle = a_A^+ a_B^+|g\rangle = c_\alpha^+ c_\beta^+|g\rangle$ due to the multipulse framework which will access it. The Hamiltonian does not account for exciton-exciton binding or repulsion terms, so the energy

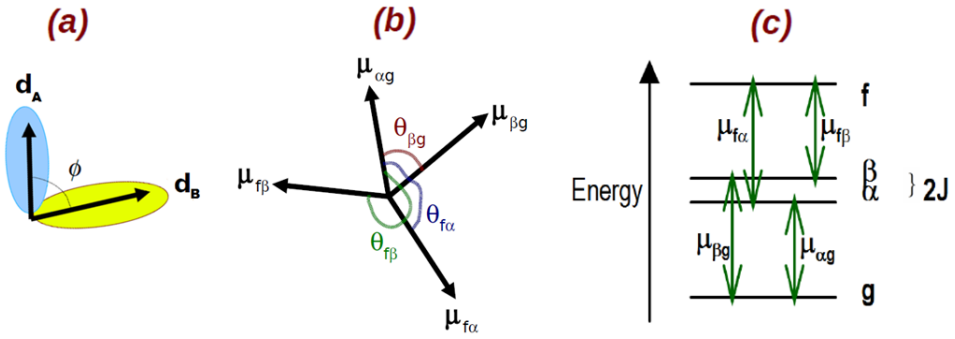

Figure 1: *Parameters of the coupled heterodimer.* (a) Dipole vectors $\boldsymbol{d}_1$ and $\boldsymbol{d}_2$ for each chromophoric site. The angle between them is ϕ. (b) Transition dipole moments between the different eigenstates of H_S. Angles are referenced with respect to $\boldsymbol{\mu}_{\alpha g}$. (c) Energy spectrum of H_S and allowed dipole transitions.

level of the biexciton is $\omega_f = \omega_\alpha + \omega_\beta = \omega_A + \omega_B$. Denoting, $\omega_{ij} \equiv \omega_i - \omega_j$, we immediately note that,

$$\begin{aligned} \omega_{\alpha g} &= \omega_{f\beta} \\ \omega_{\beta g} &= \omega_{f\alpha}. \end{aligned} \tag{5}$$

For a coupled heterodimer, the dipole moments $\boldsymbol{\mu}_{ij}$ for $i, j \in \{\alpha, \beta, f\}$ are located in the same plane, but in general have different magnitudes and directions (see Fig. 1).

We are interested in the interaction of the excitonic system S with three laser pulses:

$$V(t) = -\lambda \sum_{i=1}^{3} \hat{\boldsymbol{\mu}} \cdot \boldsymbol{e_i} E(t - t_i) e^{i\boldsymbol{k}_i \cdot \boldsymbol{r} - i\omega_i (t - t_i)} + c.c., \tag{6}$$

where λ is the intensity of the electric field, which is assumed weak, $\hat{\boldsymbol{\mu}}$ is the dipole operator, $\boldsymbol{e_i}, t_i, \boldsymbol{k}_i, \omega_i$ denote the polarization, time center, wavector, and carrier frequency of the $i-th$ pulse. $E(t)$ is the slowly varying pulse envelope, which we choose as a Gaussian with width σ, $E(t) = e^{-t^2/(2\sigma^2)}$. Four-wave mixing experiments measure the polarization induced on a chromophore at position $\boldsymbol{r}$ upon interaction with three pulses, $P(\boldsymbol{r}, t) = Tr(\mu \rho_S(t))$, which can be detected by heterodyning with a fourth electric field, named local oscillator [15]. Formally, this polarization can be Fourier decomposed along different wavectors as $P(\boldsymbol{r}, t) = \sum_s P_s(t) e^{i\boldsymbol{k}_s \cdot \boldsymbol{r}}$. Via phase matching, specific components of $P(\boldsymbol{r}, t)$ can be monitored. We shall be interested in the photon-echo (PE) component $P_{PE}(t)$ corresponding to $\boldsymbol{k}_{PE} = -\boldsymbol{k}_1 + \boldsymbol{k}_2 + \boldsymbol{k_3}$.

In the following section, we present the main results of our study. We show that a series of two-color rephasing PE experiments on a coupled heterodimer can be conceptually regarded as a QPT of the first exciton manifold (see Fig. 2). We demonstrate that the preparation of a complete set that spans the single exciton manifold is achieved by applying all the possible combinations of two different central frequencies in the first two pulses centered at t_1 and t_2 which, in the terminology of PE experiments, define the so-colled *coherence time* interval $\tau = t_2 - t_1$. The time interval between the center of the second and third pulses, called the *waiting time* $T = t_3 - t_2$, delimit the quantum channel [18] which we want to characterize by QPT. Finally, we carry out QST of the resulting second order density matrix at the instant $t = t_3 = 0$, which we regard as the origin of the timeline t. This task is indirectly performed by first acting a third pulse to generate new coherences which are dipole active and then heterodyning the polarization along $\boldsymbol{k}_{PE}$ at t_4, that is, after the *echo time* $t_4 - t_3$ has elapsed. As we shall explain in detail, this polarization can be expressed as a linear combination of elements of the second order density matrix. In fact, the realization of a set of PE experiments varying the third pulse central frequency between the same two colors used in the first pulses, and alternating between two pulse polarization schemes, yield enough linear equations to extract each of the elements of this second order density matrix. Besides this study, we shall comment on possibilities to constrain the QPT with additional data routinely collected in PE experiments.

Results

To make the discussion more concrete, we adapt the parameters in the experiment of Lee and coworkers which probes the special pair in the reaction center of the *Rhodobacter sphaeroides* bacteria *[29]* ($\omega_1 = 12945\,cm^{-1}$, $\omega_2 = 12655\,cm^{-1}$, $J = 220\,cm^{-1}$) and employs pulses of two central wavelengths, 750 and 850 nm, which correspond to the carrier frequencies $\omega_+ = 13333\,cm^{-1}$ and $\omega_- = 12500\,cm^{-1}$. We choose the width of the pulse to be $\sigma = 40\,fs$. The duration is short enough that it creates amplitudes in both single-exciton states, but predominantly excite $|\alpha\rangle$ or $|\beta\rangle$, respectively. Our goal is not to reproduce the dynamics of this particular excitonic system, but to illustrate the QPT protocol.

Presumably, a "cleaner" scheme would employ longer pulses so that in frequency space they would centered about only one of the excitons at a time. However, if decoherence processes are

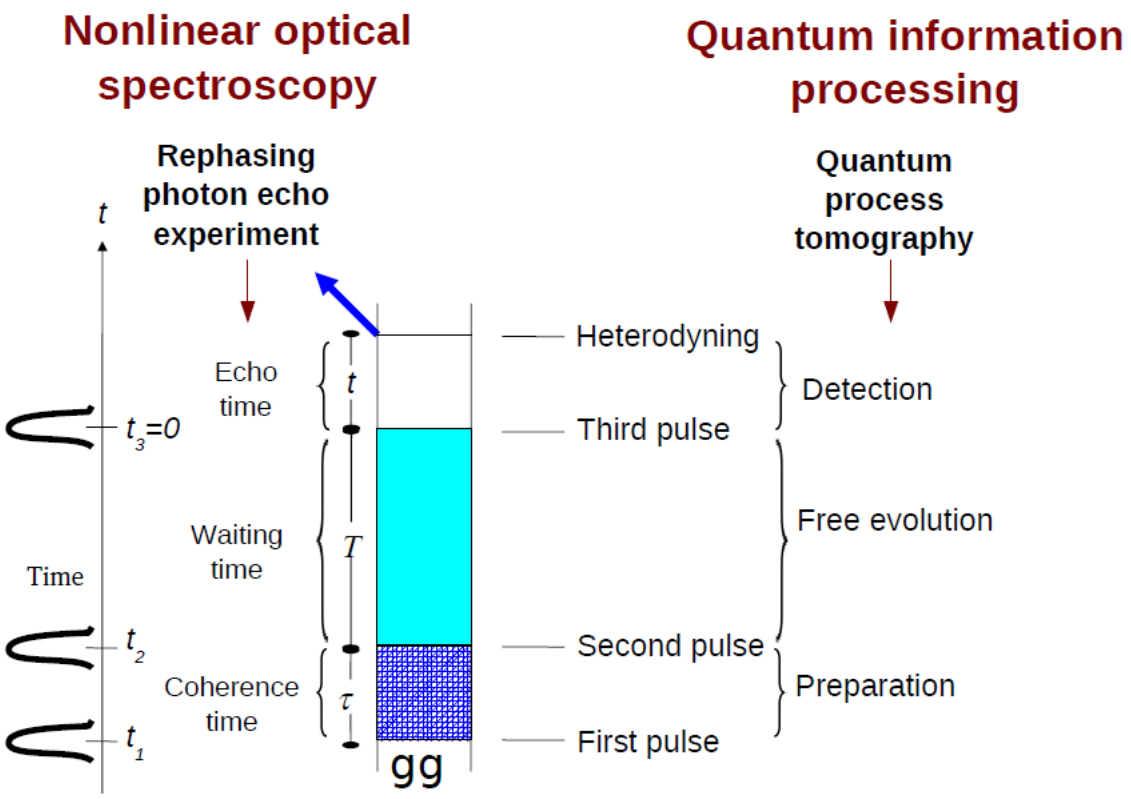

Figure 2: *Rephasing photon echo experiment seen as a quantum process tomography.* Pulses are centered about t_1, t_2, t_3. The origin of the timeline is chosen to be $t = t_3 = 0$. The first three pulses define the *coherence* (τ) and *waiting* (T) times, and the echo time is the interval t between the third pulse and the heterodyning. This experiment, in the quantum information processing language can be regarded as consisting of three stages: initial state preparation, free evolution, and detection of the output state from t_3.

fast compared to this pulse envelope time width, the target state will have disappeared by the time the envelope has ended, so that the dynamics of interest will not be explicitly monitored. The opposite scenario, the impulsive limit, is also undesirable, because indiscriminate excitation of the entire excitonic spectrum might not allow for a complete set of initial states to be prepared. The pulse parameters we have chosen satisfy both of these requirements. Also, for purposes of the QPT protocol, we assume that the parameters $\omega_{\alpha g}$, $\omega_{\beta g}$, $\boldsymbol{\mu}_{\alpha g}$, $\boldsymbol{\mu}_{\alpha g}$, $\boldsymbol{\mu}_{\alpha g}$, and $\boldsymbol{\mu}_{\alpha g}$ are all known. Information about the transition frequencies can be obtained from a linear absorption spectrum, whereas the one concerning the dipoles can be extracted from x-ray crystallography [30].

Initial state preparation.— Before any electromagnetic interaction, the excitonic system is in the ground state $\rho_S(-\infty) = |g\rangle\langle g|$. The first two pulses traveling at the $-\boldsymbol{k}_1$ and $\boldsymbol{k}_2$ directions with

respective frequencies $\omega_1, \omega_2 \in \{\omega_+, \omega_-\}$, generate a state in the chromophore that can be formally associated to a second order density matrix denoted by $[\rho^{(2)}_{-\boldsymbol{k}_1,\boldsymbol{k}_2}]^{\omega_1,\omega_2}_{\boldsymbol{e}_1,\boldsymbol{e}_2}$, where the subscripts keep track of the wavevectors and polarizations of the fields, and the superscripts indicate their central frequencies. Applying second order perturbation theory and the rotating-wave approximation (RWA), it can be shown that (see Supplementary Information):

$$[\rho^{(2)}_{-\boldsymbol{k}_1,\boldsymbol{k}_2}]^{\omega_1,\omega_2}_{\boldsymbol{e}_1,\boldsymbol{e}_2}(t_2+T) \;=\; \chi(T)\tilde{\rho}^{\omega_1,\omega_2}_{\boldsymbol{e}_1,\boldsymbol{e}_2}(0), \tag{7}$$

where we have defined the effective *initial state* prepared by the first two laser pulses as:

$$\tilde{\rho}^{\omega_1,\omega_2}_{\boldsymbol{e}_1,\boldsymbol{e}_2}(0) = -\sum_{pq} C^p_{\omega_1} C^q_{\omega_2} (\boldsymbol{\mu}_{pg}\cdot\boldsymbol{e}_1)(\boldsymbol{\mu}_{qg}\cdot\boldsymbol{e}_2)\mathcal{G}_{gp}(\tau)(|q\rangle\langle p| - \delta_{pq}|g\rangle\langle g|), \tag{8}$$

which holds for $\tau, T >\sim 3\sigma$, that is, in the case of negligible pulse overlap and after the action of the first two pulses has effectively ended. The coefficients $C^p_{\omega_i}$ for $p \in \{\alpha, \beta\}$ are frequency amplitudes of the laser pulse which is centered at ω_i, evaluated at the transition energy ω_{pg}:

$$C^p_{\omega_i} = -\frac{\lambda}{i}\sqrt{2\pi\sigma^2}e^{-\sigma^2(\omega_{pg}-\omega_i)^2/2}, \tag{9}$$

and

$$\mathcal{G}_{ij}(\tau) = \theta(\tau)e^{(-i\omega_{ij}-\Gamma_{ij})\tau} \tag{10}$$

is the propagator of the optical coherence $|i\rangle\langle j|$, which, for simplicity, has been taken to be the product of a coherent oscillatory term beating at a frequency ω_{ij} and an exponential decay with dephasing rate Γ_{ij}, assumed to be known. This propagator is defined only for $\tau > 0$ via the step function $\theta(\tau)$.

By extending the definition of $\tilde{\rho}^{\omega_1,\omega_2}_{\boldsymbol{e}_1,\boldsymbol{e}_2}(0)$ to positive times via $\tilde{\rho}^{\omega_1,\omega_2}_{\boldsymbol{e}_1,\boldsymbol{e}_2}(T) \equiv [\rho^{(2)}_{-\boldsymbol{k}_1,\boldsymbol{k}_2}]^{\omega_1,\omega_2}_{\boldsymbol{e}_1,\boldsymbol{e}_2}(t_2+T)$, equation (7) may be rewritten as:

$$\tilde{\rho}^{\omega_1,\omega_2}_{\boldsymbol{e}_1,\boldsymbol{e}_2}(T) = \chi(T)\tilde{\rho}^{\omega_1,\omega_2}_{\boldsymbol{e}_1,\boldsymbol{e}_2}(0), \tag{11}$$

which is of the form of equation (1), and therefore, appealing for our QPT purposes.

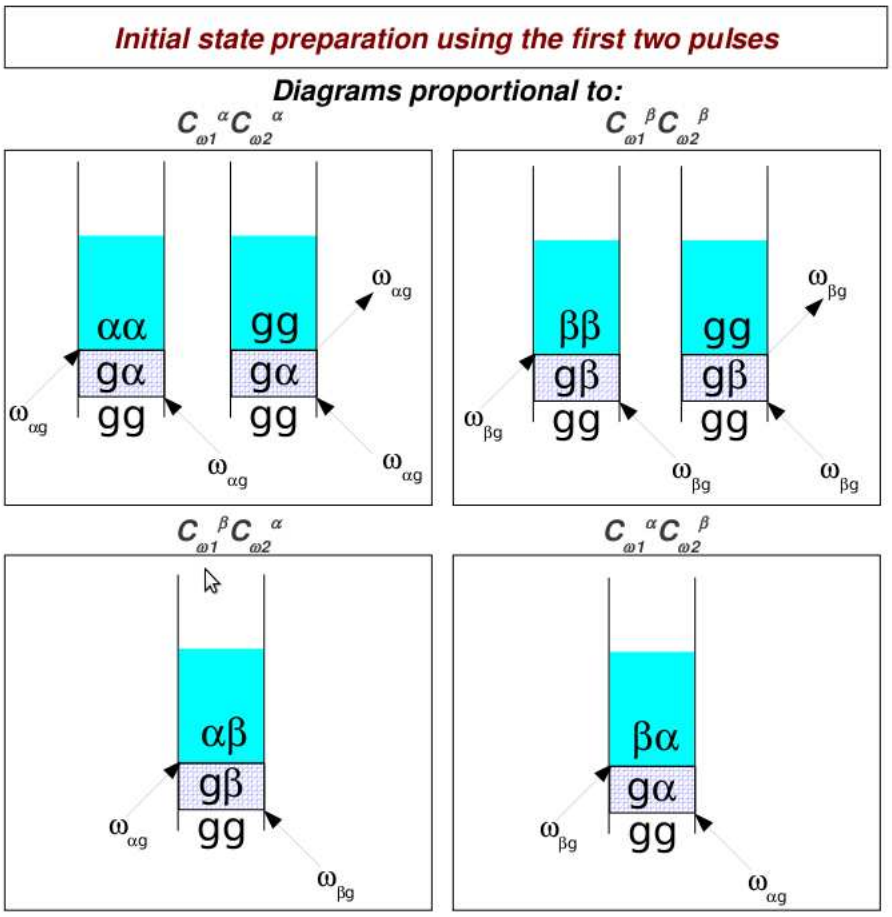

Figure 3: *Initial state preparation.* General for of the linear combination of states prepared with a single pair of pulses, each of them with center at about $\omega_1, \omega_2 \in \{\omega_+, \omega_-\}$. (There are four linearly independent initial states which can be prepared by choosing between ω_+ and ω_- twice). For example, on the bottom right panel, the state $|\alpha\rangle\langle\beta|$ is created with an ampitude proportional to $C^{\beta}_{\omega_1} C^{\alpha}_{\omega_2}$, that is, the frequency amplitude of the first pulse matching the transition energy $\omega_{\beta g}$ and the second pulse matching $\omega_{\alpha g}$. The rest of the panels can be understood analogously.

Equation (8) has a very simple interpretation, and in fact, can be easily read off from the Feynman diagrams depicted in Fig. 3. Since the initial state is $|g\rangle\langle g|$, the first pulse traveling along $-\boldsymbol{k}_1$, which is proportional to $e^{i\omega_1(t-t_1)}$, can only excite the ket in the RWA, generating an optical coherence $|g\rangle\langle p|$ with amplitude $C^{p}_{\omega_1}$. This coherence undergoes free evolution for an effective time τ under $\mathcal{G}_{gp}(\tau)$ before the next pulse at $+\boldsymbol{k}_2$ perturbs the system. This second pulse is assumed to overlap negligibly in time with the first one and is proportional to $e^{-i\omega_2(t-t_2)}$. It can act on $|g\rangle\langle p|$ on the ket to yield $|q\rangle\langle p|$ with amplitude $C^{q}_{\omega_2}$ and on the bra to create a *hole* $-|g\rangle\langle g|$ with amplitude $C^{p}_{\omega_2}$. Furthermore, the amplitude of this prepared initial state is proportional to the

alignment of the corresponding transition dipole moments with the polarization of the incoming fields. Once the initial state is prepared, it transforms via $\chi(T)$, which is the object we want to characterize.

As we already noted, the sum over p and q in equation (8) arises due to the relatively short duration of the pulses compared to the energy gap between the $|\alpha\rangle$ and $|\beta\rangle$ states, which creates not only a single coherence or population, but a linear combination of them. This is not a problem, however, as four linearly independent initial states can still be prepared by enumerating the different combinations of the initial laser pulses: $(\omega_1, \omega_2) \in \{(\omega_+, \omega_+), (\omega_+, \omega_-), (\omega_-, \omega_+), (\omega_-, \omega_-)\}$. Another possible nuisance is the contamination of the initial states by terms proportional to a hole $-|g\rangle\langle g|$ everytime there is an excited state population $|p\rangle\langle p|$. This is not a difficulty either if we assume that:

$$\chi_{abgg}(T) = \delta_{ag}\delta_{bg}, \tag{12}$$

that is, if the ground state population does not transform into any other state via free evolution. This is very reasonable if we ignore processes where phonons can induce upward optical transitions.

Evolution and measurement.— Bath induced transfers between coherences and populations can happen during the evolution after initial state preparation, and are systematically described by $\chi(T)$. For the entry gg in $\tilde{\rho}^{\omega_1,\omega_2}_{\boldsymbol{e}_1,\boldsymbol{e}_2}(0)$, we assume that it trivially transforms according to equation (12). In the general case, the rest of the initially prepared entries pq can transform into any entry $ij \in \{gg, g\alpha, g\beta, \alpha g, \alpha\alpha, \alpha\beta, \beta g, \beta\alpha, \beta\beta\}$ of $\tilde{\rho}^{\omega_1,\omega_2}_{\boldsymbol{e}_1,\boldsymbol{e}_2}(T)$. By definition, these final entries are proportional to $\chi_{ijpq}(T)$, with the exception of the gg entry, which is proportional to $\chi_{ggpq}(T) + \delta_{pq}$ due to the contamination of the hole in the initial state. We neglect the appearance of elements in entries associated with the biexciton $|f\rangle$ based on the same energy scale arguments presented in the previous paragraph.

The application of the third laser pulse with $\omega_3 \in \{\omega_+, \omega_-\}$ along $\boldsymbol{k}_3$ and centered about time $t_3 = 0$ will selectively excite certain coherences and populations. As an illustration (see Fig. 4), the component of the laser matching the transition energy $\omega_{\alpha g} = \omega_{f\beta}$ and proportional to $C^{\alpha}_{\omega_3}$ will interact with every element of $\tilde{\rho}^{\omega_1,\omega_2}_{\boldsymbol{e}_1,\boldsymbol{e}_2}$ except for αg and $\alpha\beta$, which cannot resonantly transition to any state under that particular frequency. The resulting third order density matrix will consist of a linear combination of various populations and coherences, and due to the particular model we are studying, only certain coherences will be dipole active. By keeping track of the elements of $\tilde{\rho}^{\omega_1,\omega_2}_{\boldsymbol{e}_1,\boldsymbol{e}_2}$ that yield these dipole active coherences after the third pulse, we conclude that only the entries $gg, \alpha\beta, \alpha\alpha, \beta\beta$ of $\tilde{\rho}^{\omega_1,\omega_2}_{\boldsymbol{e}_1,\boldsymbol{e}_2}(T)$ will be effectively monitored after heterodyne detection at time t. A

similar argument can be made for the laser component with energy $\omega_{\beta g} = \omega_{f\beta}$, through which only the entries $gg, \beta\alpha, \alpha\alpha, \beta\beta$ of $\tilde{\rho}^{\omega_1,\omega_2}_{\boldsymbol{e}_1,\boldsymbol{e}_2}$ will be monitored through the polarization proportional to $C^{\beta}_{\omega_3}$. With these considerations, the polarization $[P_{PE}]^{\omega_1,\omega_2,\omega_3}_{\boldsymbol{e}_1,\boldsymbol{e}_2,\boldsymbol{e}_3,\boldsymbol{e}_4}(t)$ along the photon-echo $\boldsymbol{k}_{PE}$ direction after the pulses with frequencies $\omega_1, \omega_2, \omega_3$ and polarizations $\boldsymbol{e}_1, \boldsymbol{e}_2, \boldsymbol{e}_3$, and final heterodyning at time t along polarization $\boldsymbol{e}_4$, can be expressed as:

$$[P_{PE}]^{\omega_1,\omega_2,\omega_3}_{\boldsymbol{e}_1,\boldsymbol{e}_2,\boldsymbol{e}_3,\boldsymbol{e}_4}(t) \;=\; \sum_{p,q,r} C^{p}_{\omega_1} C^{q}_{\omega_2} C^{r}_{\omega_3} P^{p,q,r}_{\boldsymbol{e}_1,\boldsymbol{e}_2,\boldsymbol{e}_3,\boldsymbol{e}_4}(t), \tag{13}$$

where,

$$\begin{aligned} P^{p,q,\alpha}_{\boldsymbol{e}_1,\boldsymbol{e}_2,\boldsymbol{e}_3,\boldsymbol{e}_4}(t) \;=\; & -(\boldsymbol{\mu}_{pg}\cdot\boldsymbol{e}_1)(\boldsymbol{\mu}_{qg}\cdot\boldsymbol{e}_2)\mathcal{G}_{gp}(\tau) \\ & \times\{[(\boldsymbol{\mu}_{\alpha g}\cdot\boldsymbol{e}_3)(\boldsymbol{\mu}_{\alpha g}\cdot\boldsymbol{e}_4)\mathcal{G}_{\alpha g}(t)(\chi_{ggqp}(T) - \delta_{pq} - \chi_{\alpha\alpha qp}(T)) \\ & +(\boldsymbol{\mu}_{f\beta}\cdot\boldsymbol{e}_3)(\boldsymbol{\mu}_{f\beta}\cdot\boldsymbol{e}_4)\mathcal{G}_{f\beta}(t)\chi_{\beta\beta qp}(T) \\ & +((\boldsymbol{\mu}_{f\beta}\cdot\boldsymbol{e}_3)(\boldsymbol{\mu}_{f\alpha}\cdot\boldsymbol{e}_4)\mathcal{G}_{f\alpha}(t) - (\boldsymbol{\mu}_{\alpha g}\cdot\boldsymbol{e}_3)(\boldsymbol{\mu}_{\beta g}\cdot\boldsymbol{e}_4)\mathcal{G}_{\beta g}(t))\chi_{\beta\alpha qp}(T)]\}, \end{aligned} \tag{14}$$

and,

$$\begin{aligned} P^{p,q,\beta}_{\boldsymbol{e}_1,\boldsymbol{e}_2,\boldsymbol{e}_3,\boldsymbol{e}_4}(t) \;=\; & -(\boldsymbol{\mu}_{pg}\cdot\boldsymbol{e}_1)(\boldsymbol{\mu}_{qg}\cdot\boldsymbol{e}_2)\mathcal{G}_{gp}(t) \\ & \times\{[(\boldsymbol{\mu}_{\beta g}\cdot\boldsymbol{e}_3)(\boldsymbol{\mu}_{\beta g}\cdot\boldsymbol{e}_4)\mathcal{G}_{\beta g}(t)(\chi_{ggqp}(T) - \delta_{pq} - \chi_{\beta\beta qp}(T)) \\ & +(\boldsymbol{\mu}_{f\alpha}\cdot\boldsymbol{e}_3)(\boldsymbol{\mu}_{f\alpha}\cdot\boldsymbol{e}_4)\mathcal{G}_{f\alpha}(t)\chi_{\alpha\alpha qp}(T) \\ & +((\boldsymbol{\mu}_{f\alpha}\cdot\boldsymbol{e}_3)(\boldsymbol{\mu}_{f\beta}\cdot\boldsymbol{e}_4)\mathcal{G}_{f\beta}(t) - (\boldsymbol{\mu}_{\beta g}\cdot\boldsymbol{e}_3)(\boldsymbol{\mu}_{\alpha g}\cdot\boldsymbol{e}_4)\mathcal{G}_{\alpha g}(t))\chi_{\alpha\beta qp}(T)]\}. \end{aligned} \tag{15}$$

Equation (13) expresses the total PE polarization $[P_{PE}]^{\omega_1,\omega_2,\omega_3}_{\boldsymbol{e}_1,\boldsymbol{e}_2,\boldsymbol{e}_3,\boldsymbol{e}_4}(t)$ as a weighted sum of PE polarizations $P^{p,q,r}_{\boldsymbol{e}_1,\boldsymbol{e}_2,\boldsymbol{e}_3,\boldsymbol{e}_4}(t)$ that would have resulted if each of the three laser pulses had definite energies ω_{pg}, ω_{qr} and ω_{rg}, respectively, just as in the hypothetical "clean" experiments we digressed about at the beginning of the section. The optical rephasing coherence propagator in the echo time is again taken to be of the simple form of equation (10) by the obvious substitution $\tau \to t$. Just as with initial state preparation, equation (13) is only valid for $t >\sim 3\sigma$. At this point, we acknowledge that a few elements $\chi_{ijqp}(T)$ for $ij \in \{g\alpha, g\beta, \alpha g, \beta g\}$ do not appear in either equation (14) or (15) for this particular model system, and therefore will not be obtained in this QPT scheme. We are currently analyzing alternative experimental schemes that could potentially yield this information.

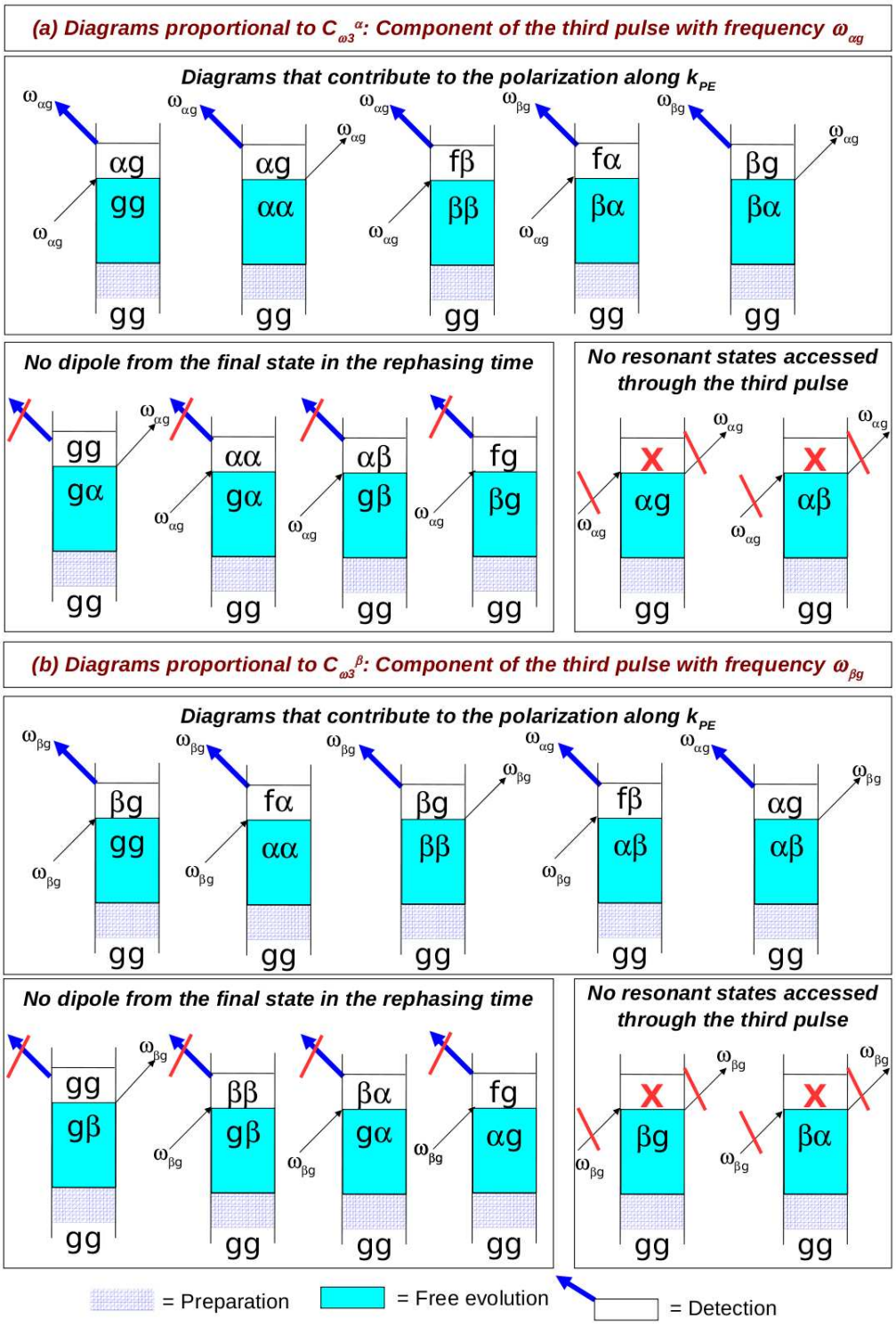

Figure 4: *Detection scheme.* (a) In the top panel, the component $C_{\omega_3}^{\alpha}$ of the third pulse, which is proportional to the frequency amplitude at the transition energy $\omega_{\alpha g}$, can selectively detect certain elements of the density matrix at t_2, that is, at the end of the waiting time, which is the quantum channel of our interest. (b) The analog scenario with $C_{\omega_3}^{\beta}$ is shown in the lower panel.

In the most typical laboratory setting, measurements are carried out from a sample of isotropically distributed chromophores. Therefore, equation (13) needs to be modified to:

$$\langle [P_{PE}]^{\omega_1,\omega_2,\omega_3}_{\boldsymbol{e}_1,\boldsymbol{e}_2,\boldsymbol{e}_3,\boldsymbol{e}_4}(t)\rangle_{iso} = \sum_{p,q,r} C^p_{\omega_1} C^q_{\omega_2} C^r_{\omega_3} \langle P^{p,q,r}_{\boldsymbol{e}_1,\boldsymbol{e}_2,\boldsymbol{e}_3,\boldsymbol{e}_4}(t)\rangle_{iso}, \tag{16}$$

where the isotropic average $\langle\cdot\rangle_{iso}$ for a tetradic $(\boldsymbol{\mu}_a\cdot\boldsymbol{e}_1)(\boldsymbol{\mu}_b\cdot\boldsymbol{e}_2)(\boldsymbol{\mu}_c\cdot\boldsymbol{e}_3)(\boldsymbol{\mu}_d\cdot\boldsymbol{e}_4)$ is given by [31]:

$$\langle(\boldsymbol{\mu}_a\cdot\boldsymbol{e}_1)(\boldsymbol{\mu}_b\cdot\boldsymbol{e}_2)(\boldsymbol{\mu}_c\cdot\boldsymbol{e}_3)(\boldsymbol{\mu}_d\cdot\boldsymbol{e}_4)\rangle_{iso} = \sum_{m_1m_2m_3m_4} I^{(4)}_{e_1e_2e_3e_4;m_1m_2m_3m_4}[(\boldsymbol{\mu}_a\cdot\boldsymbol{m}_1)(\boldsymbol{\mu}_b\cdot\boldsymbol{m}_2)(\boldsymbol{\mu}_c\cdot\boldsymbol{m}_3)(\boldsymbol{\mu}_d\cdot\boldsymbol{m}_4)], \tag{17}$$

$$I_{e_1e_2e_3e_4;m_1m_2m_3m_4} = \frac{1}{30}\left[\delta_{e_1e_2}\delta_{e_3e_4}\ \ \delta_{e_1e_3}\delta_{e_2e_4}\ \ \delta_{e_1e_4}\delta_{e_2e_3}\right]\begin{bmatrix} 4 & -1 & -1\\ -1 & 4 & -1\\ -1 & -1 & 4\end{bmatrix}\begin{bmatrix}\delta_{m_1m_2}\delta_{m_3m_4}\\ \delta_{m_1m_3}\delta_{m_2m_4}\\ \delta_{m_1m_4}\delta_{m_2m_3}\end{bmatrix}. \tag{18}$$

Suppose eight different experiments are performed by choosing each of the three pulses to be of either ω_+ or ω_- central frequency, and fixing the pulse polarization scheme at $(\boldsymbol{e}_1,\boldsymbol{e}_2,\boldsymbol{e}_3,\boldsymbol{e}_4) = (z,z,z,z)$. Equation (16) can then be inverted for each of eight polarizations $\langle P^{p,q,r}_{z,z,z,z}(t)\rangle_{iso}$ with $p,q,r\in\{\alpha,\beta\}$. The same exercise can be carried out with the scheme $(\boldsymbol{e}_1,\boldsymbol{e}_2,\boldsymbol{e}_3,\boldsymbol{e}_4) = (z,x,x,z)$ to invert the eight polarizations $\langle P^{p,q,r}_{z,x,x,z}(t)\rangle_{iso}$. In summary, these sixteen PE experiments (thirty-two heterodyne detections) yield sixteen complex polarizations of the form $\langle P^{p,q,r}_{\boldsymbol{e}_1,\boldsymbol{e}_2,\boldsymbol{e}_3,\boldsymbol{e}_4}(t)\rangle_{iso}$. Once the latter quantities are available, they can be written as linear combinations of $\chi(T)$ elements using equations (14) and (15). Another inversion step can be arranged to solve for the $\chi(T)$ elements in consideration. We refer the reader to Table 1 to elaborate on these points. By exploiting the first condition in equation (2) we can list the twenty unknowns of the $\chi(T)$ matrix to be found (see second column). Therefore, twenty algebraic conditions are required: The trace preserving condition in equation (2) yields four linear conditions, whereas the sixteen complex polarizations yield sixteen additional linear conditions (see third column). A naive approach to the problem would count two conditions per polarization, corresponding to the real and imaginary parts. However, only sixteen of these thirty-two conditions are linearly independent. These conditions can be grouped in three classes, associated with the initial state that would have been prepared in the hypothetical experiments with very long pulses (see first column). Details of the matrix equations

that accomplish the inversion of the $\chi(T)$ matrix, and therefore, the realization of QST of $\tilde{\rho}^{\omega_1,\omega_2}_{\boldsymbol{e}_1,\boldsymbol{e}_2}(T)$ and the consequent QPT, can be found in Supplementary Information. Similar polarization controlled setups have been previously suggested in the context of chirality induced signals for the Fenna-Matthews Olson (FMO) complex [32].

Example.— As an illustration, we present calculations on a secular Redfield Markovian dissipation model for the dimer. For clarity, we ignore optical dephasing or relaxation, and concentrate on the phonons. We closely follow the study reported by Fleming and coworkers [33]. Details of the calculations can be found in the Supplementary Information. The results are shown in Fig. 5. On the left, we plot the evolution of the non-zero elements of $\chi(T)$ under coherent evolution without dissipation. As expected $\chi_{\alpha\alpha\alpha\alpha}(T) = \chi_{\beta\beta\beta\beta}(T) = 1$ and $\chi_{\alpha\beta\alpha\beta}(T) = (\chi_{\beta\alpha\beta\alpha}(T))^* = e^{-i\omega_{\alpha\beta}T}$. On the right, we show the results in the presence of the Markovian dissipation. In that situation, $\chi_{\alpha\alpha\beta\beta}(T)$ becomes a small finite positive number indicating transfer of population from the higher energy state $|\beta\rangle$ to the lower energy state $|\alpha\rangle$. The consequence of this transfer is that $\chi_{\beta\beta\beta\beta}(T) \leq 1$, whereas $\chi_{\alpha\alpha\alpha\alpha}(T) = 1$ since in this system, phonons do not induce transitions from $|\alpha\rangle$ to $|g\rangle$. Furthermore, $\chi_{\alpha\beta\alpha\beta}(T)$ decays exponentially without coupling to populations or other coherences, due to the secular approximation of the model. The direct tracking of these elements can be obtained with QPT. Due to the Markovian assumption, the evolution of all the elements of the $\chi(T)$ is exponentially decreasing, which implies that QPT allows for the simple inversion of the Redfield tensor.

Discussion

In this article, we have shown how to perform QPT for a particular waiting time T for the single exciton manifold of a coupled heterodimer. Our method relies on data collected from sixteen photon-echo experimental configurations. In principle, a single and arbitrary pair of values for τ and t for each of these configurations and waiting time T is sufficient, so that only sixteen data points are needed. However, additional polarization data for many more τ and t values is routinely collected in PE settings, with this information being subsequently Fourier transformed along the different time axes and presented as multidimensional spectra [34]. The availability of this additional data presents a very interesting possibility to robustly constrain the desired information. In this context, the inversion of the $\chi(T)$ matrix would arise from taking linear combinations of

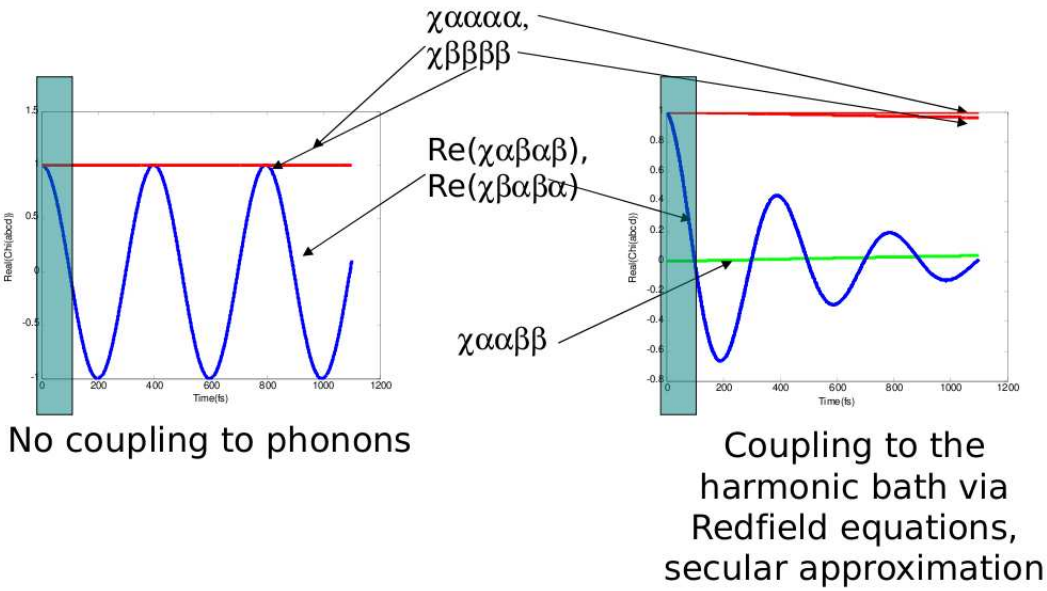

Figure 5: *Evolution of non-zero elements of* $\chi(T)$. On the left, we show the model calculation without dissipation. In such case, populations in eigenstates stay intact and coherences oscillate with a frequency that is equal to the energy gap between the states that constitute them. On the right, the calculation with Markovian dissipation under secular Redfield theory is shown. As expected, transfer of population occurs from the higher energy exciton $|\beta\rangle$ to the lower energy exciton $|\alpha\rangle$. This transfer is also accompanied by an exponential decay of the coherence elements. The blue windows in both plots represent the time interval when the envelope of the second pulse has not substantially vanished. QPT should be performed only for times T after such window.

two-dimensional spectra obtained from different pulse and polarization detection configurations, and analyzing the resulting diagonal and cross peaks. We are currently studying this alternative in relation to the possibility of extending the protocol to homodimers and reducing the number of required experimental configurations. Additionally, the lineshapes of the peaks describe the relaxation processes of the optical coherences, yielding their dephasing rates in case they are not known in anticipation (see Eq. (10)), or characterizing them in a more sophisticated manner in case they involve processes other than pure dephasing [35].

As explained, equation (1) holds if the preparation of the different initial states $\rho_S(0)$ is accompanied by a fixed $\rho_B(0)$. A dimer with a well defined vibronic structure might not satisfy this requirement, as the bath starts at different nonequilibrium configurations depending on the prepared electronic state [36–38]. In a series of very insightful papers, Cina and coworkers have

analyzed this particular scenario for purposes of nonlinear wavepacket interferometry (which can be regarded as an instance of QST for nuclear wavepackets), where two nuclear coordinates are explicitly included as part of the system, and no additional bath is considered [39–41]. A similar idea could be exploited for QPT, with the difficulty that the number of experimental resources increases exponentially with system size [42]. Ways to deal with the latter problem include compressed tomographic protocols [43, 44] or schemes that consider initial correlations between S and B [45, 46], both of which could also be potentially useful for more complex systems such as FMO. Finally, it might be worth considering additional nonlinear optical spectroscopic techniques such as transient grating [47], pump probe [1], or phase cycling of multipulse induced fluorescence [48] to investigate whether they can yield additional information for QPT.

In summary, QPT provides a very exciting framework for the study of multichromophoric systems via nonlinear optical spectroscopy in the language of quantum information processing. Further developments will surely be fueled by a close interaction with experimental groups in order to elucidate optimal ways to carry out QPT within concrete experimental constraints.

Acknowledgements

J.Y.Z. acknowledges stimulating discussions with Dr. Hohjai Lee. This work was supported by the Center of Excitonics, as an Energy Frontier Research Center funded by the US department of Energy, Office of Science, Office of Basic Energy Sciences under Award Number DESC0001088.

[1] Khalil, M., Demirdöven, N. & Tokmakoff, A. Vibrational coherence transfer characterized with fourier-transform 2d ir spectroscopy. *J. Chem. Phys.* **121**, 362–373 (2004).

[2] Stone, K. W. *et al.* Two-Quantum 2D FT Electronic Spectroscopy of Biexcitons in GaAs Quantum Wells. *Science* **324**, 1169–1173 (2009).

[3] Branigan, E. T., van Staveren, M. N. & Apkarian, V. A. Solidlike coherent vibronic dynamics in a room temperature liquid: Resonant raman and absorption spectroscopy of liquid bromine. *J. Chem. Phys.* **132**, 044503 (2010).

[4] Mukamel, S., Tanimura, Y. & Hamm, P. Coherent multidimensional optical spectroscopy. *Acc. Chem. Res.* **42**, 1207–1209 (2009).

[5] Cho, M. Coherent two-dimensional optical spectroscopy. *Chemical Reviews* **108**, 1331–1418 (2008).

[6] Engel, G. S. *et al.* Evidence for wavelike energy transfer through quantum coherence in photosynthetic systems. *Nature* **446**, 782–786 (2007).

[7] Collini, E. *et al.* Coherently wired light-harvesting in photosynthetic marine algae at ambient temperature. *Nature* **463**, 644–U69 (2010).

[8] Panitchayangkoon, G. *et al.* Long-lived quantum coherence in photosynthetic complexes at physiological temperature. *ArXiv e-prints* (2010). 1001.5108.

[9] Mohseni, M., Rebentrost, P., Lloyd, S. & Aspuru-Guzik, A. Environment-assisted quantum walks in photosynthetic energy transfer. *J. Chem. Phys.* **129**, 174106 (2008).

[10] Cao, J. & Silbey, R. J. Optimization of Exciton Trapping in Energy Transfer Processes. *J. Phys. Chem. A* **113**, 13825–13838 (2009).

[11] Olaya-Castro, A., Lee, C. F., Fassioli-Olsen, F. & Johnson, N. F. Efficiency of energy transfer in a light-harvesting system under quantum coherence. *Phys. Rev. B* **78**, 085115 (2008).

[12] Ishizaki, A. & Fleming, G. R. Theoretical examination of quantum coherence in a photosynthetic system at physiological temperature. *Proc. Natl. Acad. Sci.* **106**, 17255–17260 (2009).

[13] Sarovar M., F. G., Ishizaki A. & K.B., W. Quantum entanglement in photosynthetic light-harvesting complexes. *Nature Physics* **6**, 462 (2010).

[14] Plenio, M. B. & Huelga, S. F. Dephasing-assisted transport: quantum networks and biomolecules. *New J. Phys.* **10**, 113019 (2008).

[15] Mukamel, S. *Principles of Nonlinear Optical Spectroscopy* (Oxford, 1995).

[16] Dunn, T. J., Walmsley, I. A. & Mukamel, S. Experimental determination of the quantum-mechanical state of a molecular vibrational mode using fluorescence tomography. *Phys. Rev. Lett.* **74**, 884–887 (1995).

[17] Humble, T. S. & Cina, J. A. Molecular state reconstruction by nonlinear wave packet interferometry. *Phys. Rev. Lett.* **93**, 060402 (2004).

[18] Chuang, I. L. & Nielsen, M. A. Prescription for experimental determination of the dynamics of a quantum black box. *J. Mod. Opt.* **44**, 2455–2467 (1997).

[19] Sudarshan, E. C. G., Mathews, P. M. & Rau, J. Stochastic dynamics of quantum-mechanical systems. *Phys. Rev.* **121**, 920–924 (1961).

[20] Mohseni, M. & Lidar, D. A. Direct characterization of quantum dynamics. *Phys. Rev. Lett.* **97**, 170501 (2006).

[21] Weinstein, Y. S. *et al.* Quantum process tomography of the quantum fourier transform. *J. Chem.*

Phys. **121**, 6117–6133 (2004).

[22] Riebe, M. *et al.* Process tomography of ion trap quantum gates. *Phys. Rev. Lett.* **97**, 220407 (2006).

[23] Altepeter, J. B. *et al.* Ancilla-assisted quantum process tomography. *Phys. Rev. Lett.* **90**, 193601 (2003).

[24] Mitchell, M. W., Ellenor, C. W., Schneider, S. & Steinberg, A. M. Diagnosis, prescription, and prognosis of a bell-state filter by quantum process tomography. *Phys. Rev. Lett.* **91**, 120402 (2003).

[25] Howard, M. *et al.* Quantum process tomography and linblad estimation of a solid-state qubit. *New J. Phys.* **8**, 33 (2006).

[26] Myrskog, S. H., Fox, J. K., Mitchell, M. W. & Steinberg, A. M. Quantum process tomography on vibrational states of atoms in an optical lattice. *Phys. Rev. A* **72**, 013615 (2005).

[27] Womick, J. M. & Moran, A. M. Exciton Coherence and Energy Transport in the Light-Harvesting Dimers of Allophycocyanin. *J. Phys. Chem. B* **113**, 15747–15759 (2009).

[28] Womick, J. M. & Moran, A. M. Nature of Excited States and Relaxation Mechanisms in C-Phycocyanin. *J. Phys. Chem. B* **113**, 15771–15782 (2009).

[29] Lee, H., Cheng, Y. C. & Fleming, G. R. Coherence Dynamics in Photosynthesis: Protein Protection of Excitonic Coherence. *Science* **316**, 1462–1465 (2007).

[30] Liu, Z. F. *et al.* Crystal structure of spinach major light-harvesting complex at 2.72 angstrom resolution. *Nature* **428**, 287–292 (2004).

[31] Craig, D. & Thirunamachandran, T. *Molecular quantum electrodynamics: An introduction to radiation molecule interactions* (Dover Publications, 1998).

[32] Abramavicius, D., Voronine, D. V. & Mukamel, S. Unravelling coherent dynamics and energy dissipation in photosynthetic complexes by 2D spectroscopy. *Biophys. J.* **94**, 3613–3619 (2008).

[33] Pisliakov, A. V., Mančal, T. & Fleming, G. R. Two-dimensional optical three-pulse photon echo spectroscopy. ii. signatures of coherent electronic motion and exciton population transfer in dimer two-dimensional spectra. *J. Chem. Phys.* **124**, 234505 (2006).

[34] Jonas, D. M. Two-dimensional femtosecond spectroscopy. *Ann. Rev. Phys. Chem.* **54**, 425–463 (2003).

[35] Mukamel, S. Non-markovian theory of molecular relaxation. i. vibrational relaxation and dephasing in condensed phases. *Chem. Phys.* **37**, 33 – 47 (1979).

[36] Mančal, T. *et al.* Vibrational wave packet induced oscillations in two-dimensional electronic spectra. ii. theory. *The Journal of Chemical Physics* **132**, 184515 (2010).

[37] Egorova, D., Gelin, M. F. & Domcke, W. Analysis of cross peaks in two-dimensional electronic

photon-echo spectroscopy for simple models with vibrations and dissipation. *J. Chem. Phys.* **126**, 074314 (2007).

[38] Hanna, G. & Geva, E. Multidimensional Spectra via the Mixed Quantum-Classical Liouville Method: Signatures of Nonequilibrium Dynamics. *J. Phys. Chem. B* **113**, 9278–9288 (2009).

[39] Cina, J. A., Kilin, D. S. & Humble, T. S. Wavepacket interferometry for short-time electronic energy transfer: Multidimensional optical spectroscopy in the time domain. *J. Chem. Phys.* **118**, 46–61 (2003).

[40] Biggs, J. D. & Cina, J. A. Using wave-packet interferometry to monitor the external vibrational control of electronic excitation transfer. *J. Chem. Phys.* **131**, 224101 (2009).

[41] Biggs, J. D. & Cina, J. A. Calculations of nonlinear wave-packet interferometry signals in the pump-probe limit as tests for vibrational control over electronic excitation transfer. *J. Chem. Phys.* **131**, 224302 (2009).

[42] Mohseni, M., Rezakhani, A. T. & Lidar, D. A. Quantum-process tomography: Resource analysis of different strategies. *Phys. Rev. A* **77**, 032322 (2008).

[43] López, C. C., Bendersky, A., Paz, J. P. & Cory, D. G. Progress toward scalable tomography of quantum maps using twirling-based methods and information hierarchies. *Phys. Rev. A* **81**, 062113 (2010).

[44] Shabani, A., Mohseni, M., Lloyd, S., Kosut, R. L. & Rabitz, H. Efficient estimation of nearly sparse many-body quantum hamiltonians. *ArXiv e-prints* (2010). 1002.1330.

[45] Kuah, A. M., Modi, K., Rodríguez-Rosario, C. A. & Sudarshan, E. C. G. How state preparation can affect a quantum experiment: Quantum process tomography for open systems. *Phys. Rev. A* **76**, 042113 (2007).

[46] Meier, C. & Tannor, D. J. Non-markovian evolution of the density operator in the presence of strong laser fields. *J. Chem. Phys.* **111**, 3365–3376 (1999).

[47] Collini, E. & Scholes, G. D. Coherent Intrachain Energy Migration in a Conjugated Polymer at Room Temperature. *Science* **323**, 369–373 (2009).

[48] Tekavec, P. F., Lott, G. A. & Marcus, A. H. Fluorescence-detected two-dimensional electronic coherence spectroscopy by acousto-optic phase modulation. *J. Chem. Phys.* **127**, 214307 (2007).

[49] Mančal, T. & Fleming, G. R. Probing electronic coupling in excitonically coupled heterodimer complexes by two-color three-pulse photon echoes. *J. Chem. Phys.* **121**, 10556–10565 (2004).

[50] Pollard, W. T. & Friesner, R. A. Solution of the redfield equation for the dissipative quantum

dynamics of multilevel systems. *J. Chem. Phys.* **100**, 5054–5065 (1994).

Quantum Process Tomography of Multichromophoric Systems via Ultrafast Spectroscopy

Supplementary Information

Joel Yuen-Zhou, Masoud Mohseni and Alán Aspuru-Guzik

I. DETAILS OF THE COUPLED HETERODIMER MODEL

The operators c_j^+ and c_j can be expressed in terms of the Hamiltonian of the system H_S. By defining the average of the site energies $\omega = \frac{1}{2}(\omega_A + \omega_B)$, their difference $\Delta = \frac{1}{2}(\omega_A - \omega_B)$, and the mixing angle $\theta = \frac{1}{2}\arctan\left(\frac{J}{\Delta}\right)$, it can be easily shown that $c_\alpha = \cos\theta a_A + \sin\theta a_B$, $c_\beta = -\sin\theta a_A + \cos\theta a_B$, $\omega_\alpha = \omega + \Delta\sec 2\theta$, and $\omega_\beta = \omega - \Delta\sec 2\theta$.

Since we will be concerned with the interaction of the chromophores with electromagnetic radiation, we make some remarks on the geometry of the transition dipoles (see Fig. 1). Let the independent site transition dipole moments from the ground to the single exciton be $\boldsymbol{d}_1$ and $\boldsymbol{d}_2$, respectively. The transition dipole moments for the relevant eigenenergy transitions are [49]:

$$\begin{aligned}\begin{bmatrix}\boldsymbol{\mu}_{\alpha g}\\ \boldsymbol{\mu}_{\beta g}\end{bmatrix} &= \begin{bmatrix}\cos\theta & \sin\theta\\ -\sin\theta & \cos\theta\end{bmatrix}\begin{bmatrix}\boldsymbol{d}_A\\ \boldsymbol{d}_B\end{bmatrix}\\ \begin{bmatrix}\boldsymbol{\mu}_{f\alpha}\\ \boldsymbol{\mu}_{f\beta}\end{bmatrix} &= \begin{bmatrix}\sin\theta & \cos\theta\\ \cos\theta & -\sin\theta\end{bmatrix}\begin{bmatrix}\boldsymbol{d}_A\\ \boldsymbol{d}_B\end{bmatrix}.\end{aligned} \tag{19}$$

To simplify notation, we assume that J and the components of $\boldsymbol{d}_A$ and $\boldsymbol{d}_B$ are all real, which imply that $\boldsymbol{\mu}_{ij} = \boldsymbol{\mu}_{ji}$, for all $i, j \in \{\alpha, \beta, f\}$. As explained in the article, for a coupled heterodimer, the four dipoles in equation (19) are located in the same plane, but in general have different magnitudes and directions. This is an important fact that is exploited in the protocol to yield sufficient linearly independent equations to carry out QST. Following the convention above, we label the magnitude of $\boldsymbol{\mu}_{ij}$ with μ_{ij} and the angle between $\boldsymbol{\mu}_{ij}$ and $\boldsymbol{\mu}_{\alpha g}$ with ϕ_{ij}, so that the reference is with respect to $\theta_{\alpha g} = 0$ (Fig. 1).

The different transition dipole moments can be easily expressed in terms of the angle ϕ between $\boldsymbol{d}_A$ and $\boldsymbol{d}_B$, and the mixing angle θ. We shall present these functional dependences for completeness. By working in the cartesian system where $\boldsymbol{d}_A$ and $\boldsymbol{d}_B$ span the $\hat{x}\hat{z}$ plane, and $\boldsymbol{d}_A$ points in the $\hat{z}$ direction, we may write:

$$
\begin{aligned}
\boldsymbol{d}_A &= d_A\hat{z} \\
\boldsymbol{d}_B &= (d_B\cos\phi)\hat{z} + (d_B\sin\phi)\hat{x}.
\end{aligned} \tag{20}
$$

Expressing the components of the transition dipole moments:

$$
\begin{aligned}
\boldsymbol{\mu}_{\alpha g} &= (d_B\sin\theta\sin\phi)\hat{x} + (d_A\cos\theta + d_B\sin\theta\cos\phi)\hat{z}, \\
\boldsymbol{\mu}_{\beta g} &= (d_B\cos\theta\sin\phi)\hat{x} + (-d_A\sin\theta + d_B\cos\theta\cos\phi)\hat{z}, \\
\boldsymbol{\mu}_{f\alpha} &= (d_B\cos\theta\sin\phi)\hat{x} + (d_A\sin\theta + d_B\cos\theta\cos\phi)\hat{z}, \\
\boldsymbol{\mu}_{f\beta} &= (-d_B\sin\theta\sin\phi)\hat{x} + (d_A\cos\theta - d_B\sin\theta\cos\phi)\hat{z}.
\end{aligned} \tag{21}
$$

It is straightforward to calculate the norms of these quantities:

$$
\begin{aligned}
\mu_{\alpha g}^2 &= d_B^2\sin^2\theta + d_A^2\cos^2\theta + d_A d_B\sin(2\theta)\cos\phi \\
\mu_{\beta g}^2 &= d_B^2\cos^2\theta + d_A^2\sin^2\theta - d_A d_B\sin(2\theta)\cos\phi \\
\mu_{f\alpha}^2 &= d_B^2\cos^2\theta + d_A^2\sin^2\theta + d_A d_B\sin(2\theta)\cos\theta \\
\mu_{f\beta}^2 &= d_B^2\sin^2\theta + d_A^2\cos^2\theta - d_A d_B\sin(2\theta)\cos\phi.
\end{aligned} \tag{22}
$$

Furthermore, the angles between the different transition dipole moments can be calculated via:

$$
\begin{aligned}
\cos(\phi_{ij}) &= \frac{\boldsymbol{\mu}_{\alpha g}\cdot\boldsymbol{\mu}_{ij}}{\mu_{\alpha g}\mu_{ij}}, \\
\sin(\phi_{ij}) &= \frac{|\boldsymbol{\mu}_{\alpha g}\times\boldsymbol{\mu}_{ij}|}{\mu_{\alpha g}\mu_{ij}}.
\end{aligned} \tag{23}
$$

II. DERIVATION OF EQUATION (7) IN THE ARTICLE

The second order density matrix that results after the action of the two pulses can be calculated in Liouville space as (see [15]),

$$
\begin{aligned}
&[\rho^{(2)}_{-\boldsymbol{k}_1,\boldsymbol{k}_2}]^{\omega_1,\omega_2}_{\boldsymbol{e}_1,\boldsymbol{e}_2}(t_2+T) \\
&= \left(\frac{1}{i}\right)^2\int_{-\infty}^{t_2+T}dt''\int_{-\infty}^{t''}dt'\tilde{\mathcal{G}}_2(t_2+T,t'')\tilde{\mathcal{V}}(t'')\tilde{\mathcal{G}}_1(t'',t')\tilde{\mathcal{V}}(t')\rho(-\infty),
\end{aligned} \tag{24}
$$

where $\rho(-\infty) = |g\rangle\langle g|$, or alternatively, in Liouville space notation, $\rho(-\infty) = |gg\rangle\rangle$, is the ground initial state. The perturbation superoperator is $\tilde{\mathcal{V}}(t) = \sum_{i=1}^{3} \tilde{\mathcal{V}}_i(t)$, where $\tilde{\mathcal{V}}_i(t) = [\tilde{V}_i, \cdot]$, and:

$$\begin{aligned}
\tilde{V}_1(t) &= -\lambda \hat{\boldsymbol{\mu}}^{<} \cdot \boldsymbol{e_1} E(t-t_1) e^{-i\omega_1(t-t_1)} \\
\tilde{V}_2(t) &= -\lambda \hat{\boldsymbol{\mu}}^{>} \cdot \boldsymbol{e_2} E(t-t_2) e^{i\omega_2(t-t_2)} \\
\tilde{V}_3(t) &= -\lambda \hat{\boldsymbol{\mu}}^{>} \cdot \boldsymbol{e_3} E(t-t_3) e^{i\omega_3(t-t_3)}.
\end{aligned} \tag{25}$$

These expressions conveniently adapt equation (6) of the article to account for the phase matching direction of $\boldsymbol{k}_{PE}$ and to consider the RWA, where $\hat{\boldsymbol{\mu}}^{<} = \sum_{\omega_p<\omega_q} \mu_{pq}|p\rangle\langle q|$ promotes emissions from the ket or absorptions on the bra, and $\hat{\boldsymbol{\mu}}^{>} = (\hat{\boldsymbol{\mu}}^{<})^{+}$ induces the opposite processes. If $t_2 - t_1, t_3 - t_2 >\sim 3\sigma$, the pulses are well separated, we can substitute $\tilde{\mathcal{V}}(t') = \tilde{\mathcal{V}}_1(t')$ and $\tilde{\mathcal{V}}(t'') = \tilde{\mathcal{V}}_2(t'')$ in equation (24).

Since the first pulse interacts via the operator $\hat{\boldsymbol{\mu}}^{<}$, it can only act on the bra to produce optical coherences. We assume that these coherences evolve unitarily together with a constant dephasing rate (this assumption is not necessary, but it simplies our analysis):

$$\begin{aligned}
\tilde{\mathcal{G}}_1(t'', t') &= \mathcal{G}(t''-t') \\
&= \sum_{mn} \mathcal{G}_{mn}(t''-t')|mn\rangle\rangle\langle\langle mn|, \\
\mathcal{G}_{mn}(t''-t') &= e^{(-i\omega_{mn}-\Gamma_{mn})(t''-t')},
\end{aligned} \tag{26}$$

For the evolution in the waiting time, we make the following approximation:

$$\tilde{\mathcal{G}}_2(t_2+T, t'') \approx \chi(T)\mathcal{G}(t_2-t''), \tag{27}$$

where we have formally separated the propagation of the coherence or population in the first exciton manifold with the simple form of equation (10) of the article for the short time from t'' to the center of the second pulse t_2. After time t_2, we assume the general evolution of the map $\chi(T)$. Given all these assumptions and ignoring the very negligible amplitudes created in the biexcitonic state due to the first two pulses, we can simplify equation (24) of the article by effectively considering two succesive first order perturbation calculations:

$$[\rho^{(2)}_{-\boldsymbol{k}_1,\boldsymbol{k}_2}]^{\omega_1,\omega_2}_{\boldsymbol{e}_1,\boldsymbol{e}_2}(t_2+T)$$

$$
\begin{aligned}
&= -\left(\frac{-\lambda}{i}\right)^2 \sum_{pq} \{ \int_{-\infty}^{t_2+T} dt'' \chi(T)[(|q\rangle\langle g|\boldsymbol{\mu}_{qg}\cdot\boldsymbol{e}_2)\tilde{\mathcal{G}}_{qp}(t_2-t'')\}E(t''-t_2)e^{-i\omega_2(t''-t_2)} \\
&\quad \times \int_{-\infty}^{\infty} dt' \tilde{\mathcal{G}}_{gp}(t''-t_1)\tilde{\mathcal{G}}_{gp}(t_1-t')E(t'-t_1)e^{i\omega_1(t'-t_1)}(|g\rangle\langle g|)(\boldsymbol{\mu}_{pg}\cdot\boldsymbol{e}_1|g\rangle\langle p|)] \\
&\quad - \int_{-\infty}^{t_2+T} dt'' \chi(T)[\tilde{\mathcal{G}}_{qp}(t_2-t'')\}E(t''-t_2)e^{-i\omega_2(t''-t_2)} \\
&\quad \times \int_{-\infty}^{\infty} dt' \tilde{\mathcal{G}}_{gp}(t''-t_1)\tilde{\mathcal{G}}_{gp}(t_1-t')E(t'-t_1)e^{i\omega_1(t'-t_1)}(|g\rangle\langle g|)(\boldsymbol{\mu}_{pg}\cdot\boldsymbol{e}_1|g\rangle\langle p|)(|q\rangle\langle g|\boldsymbol{\mu}_{qg}\cdot\boldsymbol{e}_2)]\} \\
&= -\left(\frac{\lambda}{i}\right)^2 \sum_{pq} (\boldsymbol{\mu}_{pg}\cdot\boldsymbol{e}_1)(\boldsymbol{\mu}_{qg}\cdot\boldsymbol{e}_2) \\
&\quad \times \int_{-\infty}^{t_2+T} dt'' \chi(T)[\tilde{\mathcal{G}}_{qp}(t_2-t'')E(t''-t_2)e^{-i\omega_2(t''-t_2)} \\
&\quad \times \int_{-\infty}^{t''} dt' \tilde{\mathcal{G}}_{gp}(t''-t_1)\tilde{\mathcal{G}}_{gp}(t_1-t')E(t'-t_1)e^{i\omega_1(t'-t_1)}](|q\rangle\langle p| - \delta_{pq}|g\rangle\langle g|) \\
&= -\left(\frac{\lambda}{i}\right)^2 \sum_{pq} (\boldsymbol{\mu}_{pg}\cdot\boldsymbol{e}_1)(\boldsymbol{\mu}_{qg}\cdot\boldsymbol{e}_2) \\
&\quad \times \chi(T)[\left(\int_{-\infty}^{\infty} ds'' \tilde{\mathcal{G}}_{qp}(-s'')E(s'')e^{-i\omega_2 s''}\tilde{\mathcal{G}}_{gp}(s'')\right)\left(\tilde{\mathcal{G}}_{gp}(t_2-t_1)\right)\left(\int_{-\infty}^{\infty} ds' \tilde{\mathcal{G}}_{gp}(-s')E(s')e^{i\omega_1 s'}\right) \\
&\quad \times (|q\rangle\langle p| - \delta_{pq}|g\rangle\langle g|)] \\
&= -\chi(T)\{\sum_{pq} C^p_{\omega_1} C^q_{\omega_2} (\boldsymbol{\mu}_{pg}\cdot\boldsymbol{e}_u)(\boldsymbol{\mu}_{qg}\cdot\boldsymbol{e}_v)\mathcal{G}_{gp}(t_2-t_1)(|q\rangle\langle p| - \delta_{pq}|g\rangle\langle g|)\}, \qquad (28)
\end{aligned}
$$

where in the last steps we changed variables from t'' to $s'' = t'' - t_2$ and from t' to $s' = t' - t_1$, and extended the upper limit of both integrals to infinity by assuming that the envelope of the pulses has significantly decayed after intervals of duration τ and t. The resulting integrals are Fourier transforms of Gaussians, which are easily evaluated. The dephasing terms (imaginary frequencies) in these integrals have been neglected by reasoning that the timescale of the action of the pulse envelope is short compared to the dynamics induced by the bath.

Equations (13), (14), and (15) of the article can be easily derived from the same considerations, by just assuming another first order perturbation step in the interaction of the chromophore with the third pulse, and taking the trace of the resulting density matrix with respect to the dipole operator $\hat{\boldsymbol{\mu}}$.

III. RECONSTRUCTION OF THE χ MATRIX

NOTE: The matrices of known quantities and parameters presented in this section can be easily reexpressed in terms of d_A, d_B, ϕ, and θ using the equations in section I of the supplementary

information. This explicit substitution has been particularly avoided for clarity and due to the length of the resulting expressions.

A. Inversion of elements $\chi_{ij\alpha\alpha}(T)$

(See Table 1, entries (1,1),(1,2), and (1,3)). After isotropically averaging Equations (14) and (15) using (18), their right hand sides can still be written as linear combinations of elements $\chi_{ijpq}(T)$. Therefore, we can see that a number of different PE experiments using different pulse frequencies and polarizations can be used to generate a linear system of equations to invert those elements. We will first consider the case $p = q = \alpha$. Due to the first constraint in Equation (2), there are only five unknowns, as listed entry (1,2) of Table 1: $\chi_{gg\alpha\alpha}(T)$, $\chi_{\alpha\alpha\alpha\alpha}(T)$, $\chi_{\beta\beta\alpha\alpha}(T)$, $\Re\{\chi_{\alpha\beta\alpha\alpha}(T)\}$, and $\Im\{\chi_{\alpha\beta\alpha\alpha}(T)\}$. The second constraint $\sum_a \chi_{aa\alpha\alpha}(T) = 1$ implies that only four other linearly independent equations are necessary to invert the unknowns, which are all real numbers. It turns out that knowledge of the four polarizations $\langle P^{\alpha,\alpha,\alpha}_{z,z,z,z}(t)\rangle_{iso}$, $\langle P^{\alpha,\alpha,\beta}_{z,z,z,z}(t)\rangle_{iso}$, $\langle P^{\alpha,\alpha,\alpha}_{x,z,z,x}(t)\rangle_{iso}$, $\langle P^{\alpha,\alpha,\beta}_{x,z,z,x}(t)\rangle_{iso}$, as listed in entry (1,3) of Table 1, is sufficient for this purpose.

Arranging this information in matrix form,

$$\mathbb{M}^{\alpha\alpha} X^{\alpha\alpha} = R^{\alpha\alpha} \tag{29}$$

where

$$X^{\alpha\alpha} = \begin{bmatrix} \chi_{gg\alpha\alpha}(T) - 1 \\ \chi_{\alpha\alpha\alpha\alpha}(T) \\ \chi_{\beta\beta\alpha\alpha}(T) \\ \Re\{\chi_{\alpha\beta\alpha\alpha}(T)\} \\ \Im\{\chi_{\alpha\beta\alpha\alpha}(T)\} \end{bmatrix} \tag{30}$$

is the vector we want to solve for (the "-1" in the first entry is due to the δ_{pq} function in Equations (14) and (15) of the article, which is related to the hole $-|g\rangle\langle g|$ produced everytime $|\alpha\rangle\langle\alpha|$ or $|\beta\rangle\langle\beta|$ is prepared), and

$$R^{\alpha\alpha} = \begin{bmatrix} \langle P^{\alpha,\alpha,\alpha}_{z,z,z,z}(t)\rangle_{iso} \\ \langle P^{\alpha,\alpha,\beta}_{z,z,z,z}(t)\rangle_{iso} \\ \langle P^{\alpha,\alpha,\alpha}_{z,x,x,z}(t)\rangle_{iso} \\ \langle P^{\alpha,\alpha,\beta}_{z,x,x,z}(t)\rangle_{iso} \\ 0 \end{bmatrix} \tag{31}$$

is the vector with the PE polarizations together with the trace preserving condition in the last entry. Finally, $\mathbb{M}^{\alpha\alpha}$ is a 5×5 matrix with entries given in Table 1.

TABLE 1. Entries of $\mathbb{M}^{\alpha\alpha}$

ROW	*COLUMN*	*VALUE*
1	1	$-\frac{1}{5}\mu_{\alpha g}^4 \mathcal{G}_{g\beta}(\tau)\mathcal{G}_{\alpha g}(t)$
1	2	$\frac{1}{5}\mu_{\alpha g}^4 \mathcal{G}_{g\beta}(\tau)\mathcal{G}_{\alpha g}(t)$
1	3	$-\frac{1}{15}\left(\cos\left(2\theta_{f\beta}\right)+2\right)\mu_{f\beta}^2\mu_{\alpha g}^2\mathcal{G}_{f\beta}(t)\mathcal{G}_{g\beta}(\tau)$
1	4	$-\mathcal{G}_{g\beta}(\tau)\left(\frac{1}{15}\left(3\cos\left(\theta_{f\alpha}\right)\cos\left(\theta_{f\beta}\right)+\sin\left(\theta_{f\alpha}\right)\sin\left(\theta_{f\beta}\right)\right)\mu_{f\alpha}\mu_{f\beta}\mu_{\alpha g}^2\mathcal{G}_{f\alpha}(t)-\frac{1}{5}\cos\left(\theta_{\beta g}\right)\mu_{\alpha g}^3\mu_{\beta g}\mathcal{G}_{\beta g}(t)\right)$
1	5	$i\mathcal{G}_{g\beta}(\tau)\left(\frac{1}{15}\left(3\cos\left(\theta_{f\alpha}\right)\cos\left(\theta_{f\beta}\right)+\sin\left(\theta_{f\alpha}\right)\sin\left(\theta_{f\beta}\right)\right)\mu_{f\alpha}\mu_{f\beta}\mu_{\alpha g}^2\mathcal{G}_{f\alpha}(t)-\frac{1}{5}\cos\left(\theta_{\beta g}\right)\mu_{\alpha g}^3\mu_{\beta g}\mathcal{G}_{\beta g}(t)\right)$
2	1	$-\frac{1}{15}\left(\cos\left(2\theta_{\beta g}\right)+2\right)\mu_{\alpha g}^2\mu_{\beta g}^2\mathcal{G}_{g\beta}(\tau)\mathcal{G}_{\beta g}(t)$
2	2	$-\frac{1}{15}\left(\cos\left(2\theta_{f\alpha}\right)+2\right)\mu_{f\alpha}^2\mu_{\alpha g}^2\mathcal{G}_{f\alpha}(t)\mathcal{G}_{g\beta}(\tau)$
2	3	$\frac{1}{15}\left(\cos\left(2\theta_{\beta g}\right)+2\right)\mu_{\alpha g}^2\mu_{\beta g}^2\mathcal{G}_{g\beta}(\tau)\mathcal{G}_{\beta g}(t)$
2	4	$-\mathcal{G}_{g\beta}(\tau)\left(\frac{1}{15}\left(3\cos\left(\theta_{f\alpha}\right)\cos\left(\theta_{f\beta}\right)+\sin\left(\theta_{f\alpha}\right)\sin\left(\theta_{f\beta}\right)\right)\mu_{f\alpha}\mu_{f\beta}\mu_{\alpha g}^2\mathcal{G}_{f\beta}(t)-\frac{1}{5}\cos\left(\theta_{\beta g}\right)\mu_{\alpha g}^3\mu_{\beta g}\mathcal{G}_{\alpha g}(t)\right)$
2	5	$-i\mathcal{G}_{g\beta}(\tau)\left(\frac{1}{15}\left(3\cos\left(\theta_{f\alpha}\right)\cos\left(\theta_{f\beta}\right)+\sin\left(\theta_{f\alpha}\right)\sin\left(\theta_{f\beta}\right)\right)\mu_{f\alpha}\mu_{f\beta}\mu_{\alpha g}^2\mathcal{G}_{f\beta}(t)-\frac{1}{5}\cos\left(\theta_{\beta g}\right)\mu_{\alpha g}^3\mu_{\beta g}\mathcal{G}_{\alpha g}(t)\right)$
3	1	$-\frac{1}{15}\mu_{\alpha g}^4 \mathcal{G}_{g\beta}(\tau)\mathcal{G}_{\alpha g}(t)$
3	2	$\frac{1}{15}\mu_{\alpha g}^4 \mathcal{G}_{g\beta}(\tau)\mathcal{G}_{\alpha g}(t)$
3	3	$\frac{1}{30}\left(\cos\left(2\theta_{f\beta}\right)-3\right)\mu_{f\beta}^2\mu_{\alpha g}^2\mathcal{G}_{f\beta}(t)\mathcal{G}_{g\beta}(\tau)$
3	4	$-\mathcal{G}_{g\beta}(\tau)\left(\frac{1}{15}\left(\cos\left(\theta_{f\alpha}\right)\cos\left(\theta_{f\beta}\right)+2\sin\left(\theta_{f\alpha}\right)\sin\left(\theta_{f\beta}\right)\right)\mu_{f\alpha}\mu_{f\beta}\mu_{\alpha g}^2\mathcal{G}_{f\beta}(t)-\frac{1}{15}\cos\left(\theta_{\beta g}\right)\mu_{\alpha g}^3\mu_{\beta g}\mathcal{G}_{\beta g}(t)\right)$
3	5	$i\mathcal{G}_{g\beta}(\tau)\left(\frac{1}{15}\left(\cos\left(\theta_{f\alpha}\right)\cos\left(\theta_{f\beta}\right)+2\sin\left(\theta_{f\alpha}\right)\sin\left(\theta_{f\beta}\right)\right)\mu_{f\alpha}\mu_{f\beta}\mu_{\alpha g}^2\mathcal{G}_{f\beta}(t)-\frac{1}{15}\cos\left(\theta_{\beta g}\right)\mu_{\alpha g}^3\mu_{\beta g}\mathcal{G}_{\beta g}(t)\right)$
4	1	$\frac{1}{30}\left(\cos\left(2\theta_{\beta g}\right)-3\right)\mu_{\alpha g}^2\mu_{\beta g}^2\mathcal{G}_{g\beta}(\tau)\mathcal{G}_{\beta g}(t)$
4	2	$\frac{1}{30}\left(\cos\left(2\theta_{f\alpha}\right)-3\right)\mu_{f\alpha}^2\mu_{\alpha g}^2\mathcal{G}_{f\alpha}(t)\mathcal{G}_{g\beta}(\tau)$
4	3	$-\frac{1}{30}\left(\cos\left(2\theta_{\beta g}\right)-3\right)\mu_{\alpha g}^2\mu_{\beta g}^2\mathcal{G}_{g\beta}(\tau)\mathcal{G}_{\beta g}(t)$
4	4	$-\mathcal{G}_{g\beta}(\tau)\left(\frac{1}{15}\left(\cos\left(\theta_{f\alpha}\right)\cos\left(\theta_{f\beta}\right)+2\sin\left(\theta_{f\alpha}\right)\sin\left(\theta_{f\beta}\right)\right)\mu_{f\alpha}\mu_{f\beta}\mu_{\alpha g}^2\mathcal{G}_{f\beta}(t)-\frac{1}{15}\cos\left(\theta_{\beta g}\right)\mu_{\alpha g}^3\mu_{\beta g}\mathcal{G}_{\alpha g}(t)\right)$
4	5	$-i\mathcal{G}_{g\beta}(\tau)\left(\frac{1}{15}\left(\cos\left(\theta_{f\alpha}\right)\cos\left(\theta_{f\beta}\right)+2\sin\left(\theta_{f\alpha}\right)\sin\left(\theta_{f\beta}\right)\right)\mu_{f\alpha}\mu_{f\beta}\mu_{\alpha g}^2\mathcal{G}_{f\beta}(t)-\frac{1}{15}\cos\left(\theta_{\beta g}\right)\mu_{\alpha g}^3\mu_{\beta g}\mathcal{G}_{\alpha g}(t)\right)$
5	1	1
5	2	1
5	3	1
5	4	0
5	5	0

Notice that $X^{\alpha\alpha}$ in equation (29) is a purely real vector, whereas $\mathbb{M}^{\alpha\alpha}$ and $R^{\alpha\alpha}$ are complex in general. Defining:

$$\begin{aligned} \tilde{\mathbb{M}}^{ij} &= \begin{bmatrix} \Re\{\mathbb{M}^{ij}\} \\ \Im\{\mathbb{M}^{ij}\} \end{bmatrix}, \\ \tilde{R}^{ij} &= \begin{bmatrix} \Re\{R^{ij}\} \\ \Im\{R^{ij}\} \end{bmatrix}, \end{aligned} \tag{32}$$

we can rewrite equation (29) as:

$$\tilde{\mathbb{M}}^{\alpha\alpha} X^{\alpha\alpha} = \tilde{R}^{\alpha\alpha} \tag{33}$$

Although there are ten rows in matrix $\tilde{\mathbb{M}}$, it is of rank 5, which allows for the inversion of $X^{\alpha\alpha}$. A possible choice for five linearly independent equations is to choose rows 1,2,5 (trace condition), 8, and 9 of $\tilde{\mathbb{M}}^{\alpha\alpha}$ and $\tilde{R}^{\alpha\alpha}$, which correspond to the entries $\Re\{\langle P^{\alpha,\alpha,\alpha}_{z,z,z,z}(t)\rangle_{iso}\}$, $\Re\{\langle P^{\alpha,\alpha,\beta}_{z,z,z,z}(t)\rangle_{iso}\}$, 0, $\Im\{\langle P^{\alpha,\alpha,\alpha}_{x,z,z,x}(t)\rangle_{iso}\}$, and $\Im\{\langle P^{\alpha,\alpha,\beta}_{x,z,z,x}(t)\rangle_{iso}\}$ of $\tilde{R}^{\alpha\alpha}$. This implies that, in theory, we only need to measure the real *or* imaginary parts of the signal produced in four different photon echo experiments and use the constraint of equation (2) of the article. In pratice, however, measurement of both real and imaginary parts of the signal is routine in a heterodyne detection setting, and the additional data will allow to constraint for imperfect collection of measurements. Moreover, as mentioned in the Results part of the article, further constraining can be carried out by collecting the signal for many coherence τ and echo t times, and Fourier transforming the data in those time axes, just as in standard two-dimensional optical spectroscopy. We note that numerical tests over a wide range of parameters d_A, d_B, ϕ, and θ show that the inversion is numerically stable for a heterodimer, but is singular for the homodimer. The same situation holds for the inversion of the elements $\chi_{ij\beta\beta}$ and $\chi_{ij\alpha\beta}$, which is detailed in the next sections. This however, does not mean that other schemes could be deviced which can perform a QPT for a homodimer. As mentioned in the main text, this is currently being explored by the authors.

B. Inversion of elements $\chi_{ij\beta\beta}(T)$

(See Table 1, entries (2,1),(2,2), and (2,3)). Here we just need to replace the results of the section 2.1 above with $\alpha \to \beta$ and $\beta \to \alpha$, except for the Table 2, because of the asymmetry in the definition of the reference for the angles between the dipoles (see Fig. 1). For completeness we still present the conclusions. The matrix equation to invert is:

$$\mathbb{M}^{\beta\beta} X^{\beta\beta} = R^{\beta\beta} \tag{34}$$

where

$$X^{\beta\beta} = \begin{bmatrix} \chi_{gg\beta\beta}(T) - 1 \\ \chi_{\alpha\alpha\beta\beta}(T) \\ \chi_{\beta\beta\beta\beta}(T) \\ \Re\{\chi_{\alpha\beta\beta\beta}(T)\} \\ \Im\{\chi_{\alpha\beta\beta\beta}(T)\} \end{bmatrix} \tag{35}$$

is the column vector for unknowns and

$$R^{\beta\beta} = \begin{bmatrix} \langle P^{\beta,\beta,\alpha}_{z,z,z,z}(t)\rangle_{iso} \\ \langle P^{\beta,\beta,\beta}_{z,z,z,z}(t)\rangle_{iso} \\ \langle P^{\beta,\beta,\alpha}_{z,x,x,z}(t)\rangle_{iso} \\ \langle P^{\beta,\beta,\beta}_{z,x,x,z}(t)\rangle_{iso} \\ 0 \end{bmatrix} \tag{36}$$

is the column vector with the PE polarizations together with the trace preserving condition. Finally, $\mathbb{M}^{\beta\beta}$ is given by the entries listed in Table 2. Again, equation (34) can be split into real and imaginary parts by defining the auxiliary matrices $\tilde{\mathbb{M}}^{\beta\beta}$ and $\tilde{R}^{\beta\beta}$ according to Equation (32) to reexpress it as:

$$\tilde{\mathbb{M}}^{\beta\beta} X^{\beta\beta} = \tilde{R}^{\beta\beta} \tag{37}$$

which is a rank 5 equation, and again, equations corresponding to rows 1, 2, 5, 8, 9 of Equation (37) are a possible choice for a linearly independent set of equations.

TABLE 3. Entries of $\mathbb{M}^{\beta\beta}$

ROW	*COLUMN*	*VALUE*
1	1	$-\frac{1}{15}\mu_{\alpha g}^2(3\cos^2(\theta_{\beta g})\mu_{\beta g}^2+\sin^2(\theta_{\beta g})\mu_{\beta g}^2)\mathcal{G}_{g\alpha}(\tau)\mathcal{G}_{\alpha g}(t)$
1	2	$\frac{1}{15}\mu_{\alpha g}^2(3\cos^2(\theta_{\beta g})\mu_{\beta g}^2+\sin^2(\theta_{\beta g})\mu_{\beta g}^2)\mathcal{G}_{g\alpha}(\tau)\mathcal{G}_{\alpha g}(t)$
1	3	$-\frac{1}{15}\mu_{f\beta}^2(\sin(\theta_{\beta g})\mu_{\beta g}(\cos(\theta_{\beta g})\sin(2\theta_{f\beta})\mu_{\beta g}-(\cos(2\theta_{f\beta})-2)\sin(\theta_{\beta g})\mu_{\beta g})$ $+\cos(\theta_{\beta g})\mu_{\beta g}((\cos(2\theta_{f\beta})+2)\cos(\theta_{\beta g})\mu_{\beta g}+\sin(2\theta_{f\beta})\sin(\theta_{\beta g})\mu_{\beta g}))\mathcal{G}_{f\beta}(t)\mathcal{G}_{g\alpha}(\tau)$
1	4	$-\mathcal{G}_{g\alpha}(\tau)(\frac{1}{15}\mu_{f\alpha}\mu_{f\beta}(\sin(\theta_{\beta g})\mu_{\beta g}(\cos(\theta_{\beta g})\sin(\theta_{f\alpha}+\theta_{f\beta})\mu_{\beta g}+(\cos(\theta_{f\alpha})\cos(\theta_{f\beta})$ $+3\sin(\theta_{f\alpha})\sin(\theta_{f\beta}))\sin(\theta_{\beta g})\mu_{\beta g})+\cos(\theta_{\beta g})\mu_{\beta g}(\cos(\theta_{\beta g})(3\cos(\theta_{f\alpha})\cos(\theta_{f\beta})$ $+\sin(\theta_{f\alpha})\sin(\theta_{f\beta}))\mu_{\beta g}+\sin(\theta_{f\alpha}+\theta_{f\beta})\sin(\theta_{\beta g})\mu_{\beta g}))\mathcal{G}_{f\alpha}(t)-\frac{1}{15}\mu_{\alpha g}\mu_{\beta g}(2\cos(\theta_{\beta g})\sin^2(\theta_{\beta g})\mu_{\beta g}^2$ $+\cos(\theta_{\beta g})(3\mu_{\beta g}\cos^2(\theta_{\beta g})+\sin^2(\theta_{\beta g})\mu_{\beta g})\mu_{\beta g})\mathcal{G}_{\beta g}(t))$
1	5	$i\mathcal{G}_{g\alpha}(\tau)(\frac{1}{15}\mu_{f\alpha}\mu_{f\beta}(\sin(\theta_{\beta g})\mu_{\beta g}(\cos(\theta_{\beta g})\sin(\theta_{f\alpha}+\theta_{f\beta})\mu_{\beta g}+(\cos(\theta_{f\alpha})\cos(\theta_{f\beta})$ $+3\sin(\theta_{f\alpha})\sin(\theta_{f\beta}))\sin(\theta_{\beta g})\mu_{\beta g})+\cos(\theta_{\beta g})\mu_{\beta g}(\cos(\theta_{\beta g})(3\cos(\theta_{f\alpha})\cos(\theta_{f\beta})$ $+\sin(\theta_{f\alpha})\sin(\theta_{f\beta}))\mu_{\beta g}+\sin(\theta_{f\alpha}+\theta_{f\beta})\sin(\theta_{\beta g})\mu_{\beta g}))\mathcal{G}_{f\alpha}(t)$ $-\frac{1}{15}\mu_{\alpha g}\mu_{\beta g}(2\cos(\theta_{\beta g})\sin^2(\theta_{\beta g})\mu_{\beta g}^2+\cos(\theta_{\beta g})(3\mu_{\beta g}\cos^2(\theta_{\beta g})+\sin^2(\theta_{\beta g})\mu_{\beta g})\mu_{\beta g})\mathcal{G}_{\beta g}(t))$
2	1	$-\frac{1}{15}\mu_{\beta g}^2(\sin(\theta_{\beta g})\mu_{\beta g}(\cos(\theta_{\beta g})\sin(2\theta_{\beta g})\mu_{\beta g}-(\cos(2\theta_{\beta g})-2)\sin(\theta_{\beta g})\mu_{\beta g})$ $+\cos(\theta_{\beta g})\mu_{\beta g}(\cos(\theta_{\beta g})(\cos(2\theta_{\beta g})+2)\mu_{\beta g}+\sin(\theta_{\beta g})\sin(2\theta_{\beta g})\mu_{\beta g}))\mathcal{G}_{g\alpha}(\tau)\mathcal{G}_{\beta g}(t)$
2	2	$-\frac{1}{15}\mu_{f\alpha}^2(\sin(\theta_{\beta g})\mu_{\beta g}(\cos(\theta_{\beta g})\sin(2\theta_{f\alpha})\mu_{\beta g}-(\cos(2\theta_{f\alpha})-2)\sin(\theta_{\beta g})\mu_{\beta g})$ $+\cos(\theta_{\beta g})\mu_{\beta g}((\cos(2\theta_{f\alpha})+2)\cos(\theta_{\beta g})\mu_{\beta g}+\sin(2\theta_{f\alpha})\sin(\theta_{\beta g})\mu_{\beta g}))\mathcal{G}_{f\alpha}(t)\mathcal{G}_{g\alpha}(\tau)$
2	3	$\frac{1}{15}\mu_{\beta g}^2(\sin(\theta_{\beta g})\mu_{\beta g}(\cos(\theta_{\beta g})\sin(2\theta_{\beta g})\mu_{\beta g}-(\cos(2\theta_{\beta g})-2)\sin(\theta_{\beta g})\mu_{\beta g})$ $+\cos(\theta_{\beta g})\mu_{\beta g}(\cos(\theta_{\beta g})(\cos(2\theta_{\beta g})+2)\mu_{\beta g}+\sin(\theta_{\beta g})\sin(2\theta_{\beta g})\mu_{\beta g}))\mathcal{G}_{g\alpha}(\tau)\mathcal{G}_{\beta g}(t)$
2	4	$-\mathcal{G}_{g\alpha}(\tau)(\frac{1}{15}\mu_{f\alpha}\mu_{f\beta}(\sin(\theta_{\beta g})\mu_{\beta g}(\cos(\theta_{\beta g})\sin(\theta_{f\alpha}+\theta_{f\beta})\mu_{\beta g}$ $+(\cos(\theta_{f\alpha})\cos(\theta_{f\beta})+3\sin(\theta_{f\alpha})\sin(\theta_{f\beta}))\sin(\theta_{\beta g})\mu_{\beta g})$ $+\cos(\theta_{\beta g})\mu_{\beta g}(\cos(\theta_{\beta g})(3\cos(\theta_{f\alpha})\cos(\theta_{f\beta})+\sin(\theta_{f\alpha})\sin(\theta_{f\beta}))\mu_{\beta g}$ $+\sin(\theta_{f\alpha}+\theta_{f\beta})\sin(\theta_{\beta g})\mu_{\beta g}))\mathcal{G}_{f\beta}(t)-\frac{1}{15}\mu_{\alpha g}\mu_{\beta g}(2\cos(\theta_{\beta g})\sin^2(\theta_{\beta g})\mu_{\beta g}^2$ $+\cos(\theta_{\beta g})(3\mu_{\beta g}\cos^2(\theta_{\beta g})+\sin^2(\theta_{\beta g})\mu_{\beta g})\mu_{\beta g})\mathcal{G}_{\alpha g}(t))$
2	5	$-i\mathcal{G}_{g\alpha}(\tau)(\frac{1}{15}\mu_{f\alpha}\mu_{f\beta}(\sin(\theta_{\beta g})\mu_{\beta g}(\cos(\theta_{\beta g})\sin(\theta_{f\alpha}+\theta_{f\beta})\mu_{\beta g}$ $+(\cos(\theta_{f\alpha})\cos(\theta_{f\beta})+3\sin(\theta_{f\alpha})\sin(\theta_{f\beta}))\sin(\theta_{\beta g})\mu_{\beta g})$ $+\cos(\theta_{\beta g})\mu_{\beta g}(\cos(\theta_{\beta g})(3\cos(\theta_{f\alpha})\cos(\theta_{f\beta})+\sin(\theta_{f\alpha})\sin(\theta_{f\beta}))\mu_{\beta g}$ $+\sin(\theta_{f\alpha}+\theta_{f\beta})\sin(\theta_{\beta g})\mu_{\beta g}))\mathcal{G}_{f\beta}(t)-\frac{1}{15}\mu_{\alpha g}\mu_{\beta g}(2\cos(\theta_{\beta g})\sin^2(\theta_{\beta g})\mu_{\beta g}^2$ $+\cos(\theta_{\beta g})(3\mu_{\beta g}\cos^2(\theta_{\beta g})+\sin^2(\theta_{\beta g})\mu_{\beta g})\mu_{\beta g})\mathcal{G}_{\alpha g}(t))$
3	1	$-\frac{1}{15}\mu_{\alpha g}^2(\cos^2(\theta_{\beta g})\mu_{\beta g}^2+2\sin^2(\theta_{\beta g})\mu_{\beta g}^2)\mathcal{G}_{g\alpha}(\tau)\mathcal{G}_{\alpha g}(t)$
3	2	$\frac{1}{15}\mu_{\alpha g}^2(\cos^2(\theta_{\beta g})\mu_{\beta g}^2+2\sin^2(\theta_{\beta g})\mu_{\beta g}^2)\mathcal{G}_{g\alpha}(\tau)\mathcal{G}_{\alpha g}(t)$
3	3	$\frac{1}{30}\mu_{f\beta}^2(\sin(\theta_{\beta g})\mu_{\beta g}(\cos(\theta_{\beta g})\sin(2\theta_{f\beta})\mu_{\beta g}-(\cos(2\theta_{f\beta})+3)\sin(\theta_{\beta g})\mu_{\beta g})$ $+\cos(\theta_{\beta g})\mu_{\beta g}((\cos(2\theta_{f\beta})-3)\cos(\theta_{\beta g})\mu_{\beta g}+\sin(2\theta_{f\beta})\sin(\theta_{\beta g})\mu_{\beta g}))\mathcal{G}_{f\beta}(t)\mathcal{G}_{g\alpha}(\tau)$
3	4	$-\mathcal{G}_{g\alpha}(\tau)(-\frac{1}{30}\mu_{f\alpha}\mu_{f\beta}(\sin(\theta_{\beta g})\mu_{\beta g}(\cos(\theta_{\beta g})\sin(\theta_{f\alpha}+\theta_{f\beta})\mu_{\beta g}$ $-2(2\cos(\theta_{f\alpha})\cos(\theta_{f\beta})+\sin(\theta_{f\alpha})\sin(\theta_{f\beta}))\sin(\theta_{\beta g})\mu_{\beta g})+\cos(\theta_{\beta g})\mu_{\beta g}(\sin(\theta_{f\alpha}+\theta_{f\beta})\sin(\theta_{\beta g})\mu_{\beta g}$ $-2\cos(\theta_{\beta g})(\cos(\theta_{f\alpha})\cos(\theta_{f\beta})+2\sin(\theta_{f\alpha})\sin(\theta_{f\beta}))\mu_{\beta g}))\mathcal{G}_{f\beta}(t)$ $-\frac{1}{30}\mu_{\alpha g}\mu_{\beta g}(3\cos(\theta_{\beta g})\sin^2(\theta_{\beta g})\mu_{\beta g}^2+\cos(\theta_{\beta g})(2\cos^2(\theta_{\beta g})\mu_{\beta g}-\sin^2(\theta_{\beta g})\mu_{\beta g})\mu_{\beta g})\mathcal{G}_{\beta g}(t))$
3	5	$i\mathcal{G}_{g\alpha}(\tau)(-\frac{1}{30}\mu_{f\alpha}\mu_{f\beta}(\sin(\theta_{\beta g})\mu_{\beta g}(\cos(\theta_{\beta g})\sin(\theta_{f\alpha}+\theta_{f\beta})\mu_{\beta g}$ $-2(2\cos(\theta_{f\alpha})\cos(\theta_{f\beta})+\sin(\theta_{f\alpha})\sin(\theta_{f\beta}))\sin(\theta_{\beta g})\mu_{\beta g})+\cos(\theta_{\beta g})\mu_{\beta g}(\sin(\theta_{f\alpha}+\theta_{f\beta})\sin(\theta_{\beta g})\mu_{\beta g}$ $-2\cos(\theta_{\beta g})(\cos(\theta_{f\alpha})\cos(\theta_{f\beta})+2\sin(\theta_{f\alpha})\sin(\theta_{f\beta}))\mu_{\beta g}))\mathcal{G}_{f\beta}(t)-\frac{1}{30}\mu_{\alpha g}\mu_{\beta g}(3\cos(\theta_{\beta g})\sin^2(\theta_{\beta g})\mu_{\beta g}^2$ $+\cos(\theta_{\beta g})(2\cos^2(\theta_{\beta g})\mu_{\beta g}-\sin^2(\theta_{\beta g})\mu_{\beta g})\mu_{\beta g})\mathcal{G}_{\beta g}(t))$
4	1	$\frac{1}{30}\mu_{\beta g}^2(\sin(\theta_{\beta g})\mu_{\beta g}(\cos(\theta_{\beta g})\sin(2\theta_{\beta g})\mu_{\beta g}-(\cos(2\theta_{\beta g})+3)\sin(\theta_{\beta g})\mu_{\beta g})$ $+\cos(\theta_{\beta g})\mu_{\beta g}(\cos(\theta_{\beta g})(\cos(2\theta_{\beta g})-3)\mu_{\beta g}+\sin(\theta_{\beta g})\sin(2\theta_{\beta g})\mu_{\beta g}))\mathcal{G}_{g\alpha}(\tau)\mathcal{G}_{\beta g}(t)$
4	2	$\frac{1}{30}\mu_{f\alpha}^2(\sin(\theta_{\beta g})\mu_{\beta g}(\cos(\theta_{\beta g})\sin(2\theta_{f\alpha})\mu_{\beta g}-(\cos(2\theta_{f\alpha})+3)\sin(\theta_{\beta g})\mu_{\beta g})$ $+\cos(\theta_{\beta g})\mu_{\beta g}((\cos(2\theta_{f\alpha})-3)\cos(\theta_{\beta g})\mu_{\beta g}+\sin(2\theta_{f\alpha})\sin(\theta_{\beta g})\mu_{\beta g}))\mathcal{G}_{f\alpha}(t)\mathcal{G}_{g\alpha}(\tau)$
4	3	$-\frac{1}{30}\mu_{\beta g}^2(\sin(\theta_{\beta g})\mu_{\beta g}(\cos(\theta_{\beta g})\sin(2\theta_{\beta g})\mu_{\beta g}-(\cos(2\theta_{\beta g})+3)\sin(\theta_{\beta g})\mu_{\beta g})$ $+\cos(\theta_{\beta g})\mu_{\beta g}(\cos(\theta_{\beta g})(\cos(2\theta_{\beta g})-3)\mu_{\beta g}+\sin(\theta_{\beta g})\sin(2\theta_{\beta g})\mu_{\beta g}))\mathcal{G}_{g\alpha}(\tau)\mathcal{G}_{\beta g}(t)$
4	4	$-\mathcal{G}_{g\alpha}(\tau)(-\frac{1}{30}\mu_{f\alpha}\mu_{f\beta}(\sin(\theta_{\beta g})\mu_{\beta g}(\cos(\theta_{\beta g})\sin(\theta_{f\alpha}+\theta_{f\beta})\mu_{\beta g}$ $-2(2\cos(\theta_{f\alpha})\cos(\theta_{f\beta})+\sin(\theta_{f\alpha})\sin(\theta_{f\beta}))\sin(\theta_{\beta g})\mu_{\beta g})+\cos(\theta_{\beta g})\mu_{\beta g}(\sin(\theta_{f\alpha}+\theta_{f\beta})\sin(\theta_{\beta g})\mu_{\beta g}$ $-2\cos(\theta_{\beta g})(\cos(\theta_{f\alpha})\cos(\theta_{f\beta})+2\sin(\theta_{f\alpha})\sin(\theta_{f\beta}))\mu_{\beta g}))\mathcal{G}_{f\beta}(t)$ $-\frac{1}{30}\mu_{\alpha g}\mu_{\beta g}(3\cos(\theta_{\beta g})\sin^2(\theta_{\beta g})\mu_{\beta g}^2+\cos(\theta_{\beta g})(2\cos^2(\theta_{\beta g})\mu_{\beta g}-\sin^2(\theta_{\beta g})\mu_{\beta g})\mu_{\beta g})\mathcal{G}_{\alpha g}(t))$
4	5	$-i\mathcal{G}_{g\alpha}(\tau)(-\frac{1}{30}\mu_{f\alpha}\mu_{f\beta}(\sin(\theta_{\beta g})\mu_{\beta g}(\cos(\theta_{\beta g})\sin(\theta_{f\alpha}+\theta_{f\beta})\mu_{\beta g}-2(2\cos(\theta_{f\alpha})\cos(\theta_{f\beta})$ $+\sin(\theta_{f\alpha})\sin(\theta_{f\beta}))\sin(\theta_{\beta g})\mu_{\beta g})+\cos(\theta_{\beta g})\mu_{\beta g}(\sin(\theta_{f\alpha}+\theta_{f\beta})\sin(\theta_{\beta g})\mu_{\beta g}$ $-2\cos(\theta_{\beta g})(\cos(\theta_{f\alpha})\cos(\theta_{f\beta})+2\sin(\theta_{f\alpha})\sin(\theta_{f\beta}))\mu_{\beta g}))\mathcal{G}_{f\beta}(t)$ $-\frac{1}{30}\mu_{\alpha g}\mu_{\beta g}(3\cos(\theta_{\beta g})\sin^2(\theta_{\beta g})\mu_{\beta g}^2+\cos(\theta_{\beta g})(2\cos^2(\theta_{\beta g})\mu_{\beta g}-\sin^2(\theta_{\beta g})\mu_{\beta g})\mu_{\beta g})\mathcal{G}_{\alpha g}(t))$
5	1	1
5	2	1
5	3	1
5	4	0
5	5	0

C. Inversion of elements $\chi_{ij\alpha\beta}(T)$

(See Table 1, entries (3,1),(3,2), and (3,3)). The same exercise of section 2.1 and 2.2 with equations (14), (15), and (18) of the article needs to be performed here, except that twice, with $p = \beta, q = \alpha$ and with $p = \alpha, q = \beta$. Another important observation is that since $\chi_{aa\alpha\beta}$ is in general complex, as opposed to the $\chi_{aa\alpha\alpha}(T)$ and $\chi_{aa\beta\beta}(T)$, which are purely real, the constraint $\sum_a \chi_{aa\alpha\beta}(T) = 0$ consists of two independent equations, for the real and imaginary parts, respectively.

The result is:

$$\mathbb{M}^{\alpha\beta} X^{\alpha\beta} = R^{\alpha\beta}, \tag{38}$$

where

$$X^{\alpha\beta} = \begin{bmatrix} \Re\{\chi_{gg\alpha\beta}(T)\} \\ \Im\{\chi_{gg\alpha\beta}(T)\} \\ \Re\{\chi_{\alpha\alpha\alpha\beta}(T)\} \\ \Im\{\chi_{\alpha\alpha\alpha\beta}(T)\} \\ \Re\{\chi_{\beta\beta\alpha\beta}(T)\} \\ \Im\{\chi_{\beta\beta\alpha\beta}(T)\} \\ \Re\{\chi_{\alpha\beta\alpha\beta}(T)\} \\ \Im\{\chi_{\alpha\beta\alpha\beta}(T)\} \\ \Re\{\chi_{\beta\alpha\alpha\beta}(T)\} \\ \Im\{\chi_{\beta\alpha\alpha\beta}(T)\} \end{bmatrix} \tag{39}$$

is the column vector for unknowns of the $\chi(T)$ matrix and

$$R^{\alpha\beta} = \begin{bmatrix} \langle P^{\beta,\alpha,\alpha}_{z,z,z,z}(t)\rangle_{iso} \\ \langle P^{\beta,\alpha,\beta}_{z,z,z,z}(t)\rangle_{iso} \\ \langle P^{\beta,\alpha,\alpha}_{z,x,x,z}(t)\rangle_{iso} \\ \langle P^{\beta,\alpha,\beta}_{z,x,x,z}(t)\rangle_{iso} \\ \langle P^{\alpha,\beta,\alpha}_{z,z,z,z}(t)\rangle_{iso} \\ \langle P^{\alpha,\beta,\beta}_{z,z,z,z}(t)\rangle_{iso} \\ \langle P^{\alpha,\beta,\alpha}_{z,x,x,z}(t)\rangle_{iso} \\ \langle P^{\alpha,\beta,\beta}_{z,x,x,z}(t)\rangle_{iso} \\ 0 \\ 0 \end{bmatrix} \tag{40}$$

is the column vector with the PE polarizations together with the two trace preserving conditions. Just as in the previous sections, equation (38) can be split into real and imaginary parts by defining the auxiliary matrices $\tilde{\mathbb{M}}^{\alpha\beta}$ and $\tilde{R}^{\alpha\beta}$ according to equation (32) to reexpress it as:

$$\tilde{\mathbb{M}}^{\alpha\beta} X^{\alpha\beta} = \tilde{R}^{\alpha\beta} \tag{41}$$

which is a rank 10 equation. Rows 1, 2, 3, 4, 9 (real part of the trace condition), 10 (imaginary part of the trace condition), 15, 16, 17, and 18 of equation (41) are a possible set of of linearly independent equations, which correspond to $\Re\{\langle P^{\beta,\alpha,\alpha}_{z,z,z,z}(t)\rangle_{iso}\}$, $\Re\{\langle P^{\beta,\alpha,\beta}_{z,z,z,z}(t)\rangle_{iso}\}$, $\Re\{\langle P^{\beta,\alpha,\alpha}_{z,x,x,z}(t)\rangle_{iso}\}$, $\Re\{\langle P^{\beta,\alpha,\beta}_{z,x,x,z}(t)\rangle_{iso}\}$, 0, 0, $\Im\{\langle P^{\alpha,\beta,\alpha}_{z,z,z,z}(t)\rangle_{iso}\}$, $\Im\{\langle P^{\alpha,\beta,\beta}_{z,z,z,z}(t)\rangle_{iso}\}$, $\Im\{\langle P^{\alpha,\beta,\alpha}_{z,x,x,z}(t)\rangle_{iso}\}$, $\Im\{\langle P^{\alpha,\beta,\beta}_{z,x,x,z}(t)\rangle_{iso}\}$ of $\tilde{R}^{\alpha\beta}$, that is, eight different experiments measuring either the real or the imaginary parts of eight different PE experiments together with the two trace preserving conditions. Again, in practice the sixteen data points will be routinely taken and additional data constraining in the form of two-dimensional optical spectra will allow for a robust QPT.

TABLE 4. Entries of $\mathbb{M}^{\alpha\beta}$

ROW	*COLUMN*	*VALUE*
1	1	$-\frac{1}{5}\cos(\theta_{\beta g})\mu_{\alpha g}^3\mu_{\beta g}\mathcal{G}_{g\beta}(\tau)\mathcal{G}_{\alpha g}(t)$
1	2	$-\frac{1}{5}i\cos(\theta_{\beta g})\mu_{\alpha g}^3\mu_{\beta g}\mathcal{G}_{g\beta}(\tau)\mathcal{G}_{\alpha g}(t)$
1	3	$\frac{1}{5}\cos(\theta_{\beta g})\mu_{\alpha g}^3\mu_{\beta g}\mathcal{G}_{g\beta}(\tau)\mathcal{G}_{\alpha g}(t)$
1	4	$\frac{1}{5}i\cos(\theta_{\beta g})\mu_{\alpha g}^3\mu_{\beta g}\mathcal{G}_{g\beta}(\tau)\mathcal{G}_{\alpha g}(t)$
1	5	$-\frac{1}{15}\mu_{f\beta}^2((\cos(2\theta_{f\beta})+2)\cos(\theta_{\beta g})\mu_{\alpha g}\mu_{\beta g}+\sin(2\theta_{f\beta})\sin(\theta_{\beta g})\mu_{\alpha g}\mu_{\beta g})\mathcal{G}_{f\beta}(t)\mathcal{G}_{g\beta}(\tau)$
1	6	0
1	7	0
1	8	0
1	9	0
1	10	0
2	1	$-\frac{1}{15}\mu_{\beta g}^2(\cos(\theta_{\beta g})(\cos(2\theta_{\beta g})+2)\mu_{\alpha g}\mu_{\beta g}+\sin(\theta_{\beta g})\sin(2\theta_{\beta g})\mu_{\alpha g}\mu_{\beta g})\mathcal{G}_{g\beta}(\tau)\mathcal{G}_{\beta g}(t)$
2	2	$-\frac{1}{15}i\mu_{\beta g}^2(\cos(\theta_{\beta g})(\cos(2\theta_{\beta g})+2)\mu_{\alpha g}\mu_{\beta g}+\sin(\theta_{\beta g})\sin(2\theta_{\beta g})\mu_{\alpha g}\mu_{\beta g})\mathcal{G}_{g\beta}(\tau)\mathcal{G}_{\beta g}(t)$
2	3	$-\frac{1}{15}\mu_{f\alpha}^2((\cos(2\theta_{f\alpha})+2)\cos(\theta_{\beta g})\mu_{\alpha g}\mu_{\beta g}+\sin(2\theta_{f\alpha})\sin(\theta_{\beta g})\mu_{\alpha g}\mu_{\beta g})\mathcal{G}_{f\alpha}(t)\mathcal{G}_{g\beta}(\tau)$
2	4	$-\frac{1}{15}i\mu_{f\alpha}^2((\cos(2\theta_{f\alpha})+2)\cos(\theta_{\beta g})\mu_{\alpha g}\mu_{\beta g}+\sin(2\theta_{f\alpha})\sin(\theta_{\beta g})\mu_{\alpha g}\mu_{\beta g})\mathcal{G}_{f\alpha}(t)\mathcal{G}_{g\beta}(\tau)$
2	5	$\frac{1}{15}\mu_{\beta g}^2(\cos(\theta_{\beta g})(\cos(2\theta_{\beta g})+2)\mu_{\alpha g}\mu_{\beta g}+\sin(\theta_{\beta g})\sin(2\theta_{\beta g})\mu_{\alpha g}\mu_{\beta g})\mathcal{G}_{g\beta}(\tau)\mathcal{G}_{\beta g}(t)$
2	6	0
2	7	0
2	8	0
2	9	0
2	10	0
3	1	$-\frac{1}{15}\cos(\theta_{\beta g})\mu_{\alpha g}^3\mu_{\beta g}\mathcal{G}_{g\beta}(\tau)\mathcal{G}_{\alpha g}(t)$
3	2	$-\frac{1}{15}i\cos(\theta_{\beta g})\mu_{\alpha g}^3\mu_{\beta g}\mathcal{G}_{g\beta}(\tau)\mathcal{G}_{\alpha g}(t)$
3	3	$\frac{1}{15}\cos(\theta_{\beta g})\mu_{\alpha g}^3\mu_{\beta g}\mathcal{G}_{g\beta}(\tau)\mathcal{G}_{\alpha g}(t)$
3	4	$\frac{1}{15}i\cos(\theta_{\beta g})\mu_{\alpha g}^3\mu_{\beta g}\mathcal{G}_{g\beta}(\tau)\mathcal{G}_{\alpha g}(t)$
3	5	$-\frac{1}{60}\mu_{f\beta}^2((3\cos(2\theta_{f\beta})+1)\cos(\theta_{\beta g})\mu_{\alpha g}\mu_{\beta g}+3\sin(2\theta_{f\beta})\sin(\theta_{\beta g})\mu_{\alpha g}\mu_{\beta g})\mathcal{G}_{f\beta}(t)\mathcal{G}_{g\beta}(\tau)$
3	6	0
3	7	0
3	8	0
3	9	0
3	10	0
4	1	$-\frac{1}{60}\mu_{\beta g}^2(\cos(\theta_{\beta g})(3\cos(2\theta_{\beta g})+1)\mu_{\alpha g}\mu_{\beta g}+3\sin(\theta_{\beta g})\sin(2\theta_{\beta g})\mu_{\alpha g}\mu_{\beta g})\mathcal{G}_{g\beta}(\tau)\mathcal{G}_{\beta g}(t)$
4	2	$-\frac{1}{60}i\mu_{\beta g}^2(\cos(\theta_{\beta g})(3\cos(2\theta_{\beta g})+1)\mu_{\alpha g}\mu_{\beta g}+3\sin(\theta_{\beta g})\sin(2\theta_{\beta g})\mu_{\alpha g}\mu_{\beta g})\mathcal{G}_{g\beta}(\tau)\mathcal{G}_{\beta g}(t)$
4	3	$-\frac{1}{60}\mu_{f\alpha}^2((3\cos(2\theta_{f\alpha})+1)\cos(\theta_{\beta g})\mu_{\alpha g}\mu_{\beta g}+3\sin(2\theta_{f\alpha})\sin(\theta_{\beta g})\mu_{\alpha g}\mu_{\beta g})\mathcal{G}_{f\alpha}(t)\mathcal{G}_{g\beta}(\tau)$
4	4	$-\frac{1}{60}i\mu_{f\alpha}^2((3\cos(2\theta_{f\alpha})+1)\cos(\theta_{\beta g})\mu_{\alpha g}\mu_{\beta g}+3\sin(2\theta_{f\alpha})\sin(\theta_{\beta g})\mu_{\alpha g}\mu_{\beta g})\mathcal{G}_{f\alpha}(t)\mathcal{G}_{g\beta}(\tau)$
4	5	$\frac{1}{60}\mu_{\beta g}^2(\cos(\theta_{\beta g})(3\cos(2\theta_{\beta g})+1)\mu_{\alpha g}\mu_{\beta g}+3\sin(\theta_{\beta g})\sin(2\theta_{\beta g})\mu_{\alpha g}\mu_{\beta g})\mathcal{G}_{g\beta}(\tau)\mathcal{G}_{\beta g}(t)$
4	6	0
4	7	0
4	8	0
4	9	0
4	10	0
5	1	$-\frac{1}{5}\cos(\theta_{\beta g})\mu_{\alpha g}^3\mu_{\beta g}\mathcal{G}_{g\alpha}(\tau)\mathcal{G}_{\alpha g}(t)$
5	2	$\frac{1}{5}i\cos(\theta_{\beta g})\mu_{\alpha g}^3\mu_{\beta g}\mathcal{G}_{g\alpha}(\tau)\mathcal{G}_{\alpha g}(t)$
5	3	$\frac{1}{5}\cos(\theta_{\beta g})\mu_{\alpha g}^3\mu_{\beta g}\mathcal{G}_{g\alpha}(\tau)\mathcal{G}_{\alpha g}(t)$
5	4	$-\frac{1}{5}i\cos(\theta_{\beta g})\mu_{\alpha g}^3\mu_{\beta g}\mathcal{G}_{g\alpha}(\tau)\mathcal{G}_{\alpha g}(t)$
5	5	$-\frac{1}{15}\mu_{f\beta}^2\mu_{\alpha g}((\cos(2\theta_{f\beta})+2)\cos(\theta_{\beta g})\mu_{\beta g}+\sin(2\theta_{f\beta})\sin(\theta_{\beta g})\mu_{\beta g})\mathcal{G}_{f\beta}(t)\mathcal{G}_{g\alpha}(\tau)$
5	6	0
5	7	0
5	8	0
5	9	0
5	10	0

TABLE 4. Entries of $\mathbb{M}^{\alpha\beta}$ (continuation)

ROW	*COLUMN*	*VALUE*
6	1	$-\frac{1}{15}\mu_{\alpha g}\mu_{\beta g}^2(\cos(\theta_{\beta g})(\cos(2\theta_{\beta g})+2)\mu_{\beta g}+\sin(\theta_{\beta g})\sin(2\theta_{\beta g})\mu_{\beta g})\mathcal{G}_{g\alpha}(\tau)\mathcal{G}_{\beta g}(t)$
6	2	$\frac{1}{15}i\mu_{\alpha g}\mu_{\beta g}^2(\cos(\theta_{\beta g})(\cos(2\theta_{\beta g})+2)\mu_{\beta g}+\sin(\theta_{\beta g})\sin(2\theta_{\beta g})\mu_{\beta g})\mathcal{G}_{g\alpha}(\tau)\mathcal{G}_{\beta g}(t)$
6	3	$-\frac{1}{15}\mu_{f\alpha}^2\mu_{\alpha g}((\cos(2\theta_{f\alpha})+2)\cos(\theta_{\beta g})\mu_{\beta g}+\sin(2\theta_{f\alpha})\sin(\theta_{\beta g})\mu_{\beta g})\mathcal{G}_{f\alpha}(t)\mathcal{G}_{g\alpha}(\tau)$
6	4	$\frac{1}{15}i\mu_{f\alpha}^2\mu_{\alpha g}((\cos(2\theta_{f\alpha})+2)\cos(\theta_{\beta g})\mu_{\beta g}+\sin(2\theta_{f\alpha})\sin(\theta_{\beta g})\mu_{\beta g})\mathcal{G}_{f\alpha}(t)\mathcal{G}_{g\alpha}(\tau)$
6	5	$\frac{1}{15}\mu_{\alpha g}\mu_{\beta g}^2(\cos(\theta_{\beta g})(\cos(2\theta_{\beta g})+2)\mu_{\beta g}+\sin(\theta_{\beta g})\sin(2\theta_{\beta g})\mu_{\beta g})\mathcal{G}_{g\alpha}(\tau)\mathcal{G}_{\beta g}(t)$
6	6	0
6	7	0
6	8	0
6	9	0
6	10	0
7	1	$-\frac{1}{15}\cos(\theta_{\beta g})\mu_{\alpha g}^3\mu_{\beta g}\mathcal{G}_{g\alpha}(\tau)\mathcal{G}_{\alpha g}(t)$
7	2	$\frac{1}{15}i\cos(\theta_{\beta g})\mu_{\alpha g}^3\mu_{\beta g}\mathcal{G}_{g\alpha}(\tau)\mathcal{G}_{\alpha g}(t)$
7	3	$\frac{1}{15}\cos(\theta_{\beta g})\mu_{\alpha g}^3\mu_{\beta g}\mathcal{G}_{g\alpha}(\tau)\mathcal{G}_{\alpha g}(t)$
7	4	$-\frac{1}{15}i\cos(\theta_{\beta g})\mu_{\alpha g}^3\mu_{\beta g}\mathcal{G}_{g\alpha}(\tau)\mathcal{G}_{\alpha g}(t)$
7	5	$-\frac{1}{60}\mu_{f\beta}^2\mu_{\alpha g}((3\cos(2\theta_{f\beta})+1)\cos(\theta_{\beta g})\mu_{\beta g}+3\sin(2\theta_{f\beta})\sin(\theta_{\beta g})\mu_{\beta g})\mathcal{G}_{f\beta}(t)\mathcal{G}_{g\alpha}(\tau)$
7	6	0
7	7	0
7	8	0
7	9	0
7	10	0
8	1	$-\frac{1}{60}\mu_{\alpha g}\mu_{\beta g}^2(\cos(\theta_{\beta g})(3\cos(2\theta_{\beta g})+1)\mu_{\beta g}+3\sin(\theta_{\beta g})\sin(2\theta_{\beta g})\mu_{\beta g})\mathcal{G}_{g\alpha}(\tau)\mathcal{G}_{\beta g}(t)$
8	2	$\frac{1}{60}i\mu_{\alpha g}\mu_{\beta g}^2(\cos(\theta_{\beta g})(3\cos(2\theta_{\beta g})+1)\mu_{\beta g}+3\sin(\theta_{\beta g})\sin(2\theta_{\beta g})\mu_{\beta g})\mathcal{G}_{g\alpha}(\tau)\mathcal{G}_{\beta g}(t)$
8	3	$-\frac{1}{60}\mu_{f\alpha}^2\mu_{\alpha g}((3\cos(2\theta_{f\alpha})+1)\cos(\theta_{\beta g})\mu_{\beta g}+3\sin(2\theta_{f\alpha})\sin(\theta_{\beta g})\mu_{\beta g})\mathcal{G}_{f\alpha}(t)\mathcal{G}_{g\alpha}(\tau)$
8	4	$\frac{1}{60}i\mu_{f\alpha}^2\mu_{\alpha g}((3\cos(2\theta_{f\alpha})+1)\cos(\theta_{\beta g})\mu_{\beta g}+3\sin(2\theta_{f\alpha})\sin(\theta_{\beta g})\mu_{\beta g})\mathcal{G}_{f\alpha}(t)\mathcal{G}_{g\alpha}(\tau)$
8	5	$\frac{1}{60}\mu_{\alpha g}\mu_{\beta g}^2(\cos(\theta_{\beta g})(3\cos(2\theta_{\beta g})+1)\mu_{\beta g}+3\sin(\theta_{\beta g})\sin(2\theta_{\beta g})\mu_{\beta g})\mathcal{G}_{g\alpha}(\tau)\mathcal{G}_{\beta g}(t)$
8	6	0
8	7	0
8	8	0
8	9	0
8	10	0
9	1	1
9	2	0
9	3	1
9	4	0
9	5	1
9	6	0
9	7	0
9	8	0
9	9	0
9	10	0
10	1	0
10	2	1
10	3	0
10	4	1
10	5	0
10	6	1
10	7	0
10	8	0
10	9	0
10	10	0

IV. REDFIELD MODEL FOR MARKOVIAN DISSIPATION

The free evolution of S and B is generated by the total Hamiltonian H_{total}:

$$H_{total} = H_S + H_B + H_{SB}$$

where H_B and H_{SB} are the Hamiltonian for B and the interaction between S and B, respectively. The environment is constituted by two independent and identically distributed Ohmic bosonic baths, each linearly coupled to a site of the dimer. In summary:

$$\begin{aligned} H_B &= \sum_{i=\alpha,\beta} \sum_x \omega_{x,i} \left(b_{x,i}^+ b_{x,i} + \frac{1}{2} \right) \\ H_{SB} &= F_\alpha |\alpha\rangle\langle\alpha| + F_\beta |\beta\rangle\langle\beta| + (F_\alpha + F_\beta)|f\rangle\langle f| \\ F_i &= \sum_x \lambda_{x,i} (b_{x,i} + b_{x,i}^+) \end{aligned} \tag{42}$$

where $b_{x,i}$, $b_{x,i}^+$ are the anhilation and creation operators of the bath mode x coupled to the site i, $\lambda_{x,i}$ is a coupling strength, and the spectral density is the same for both sites:

$$\begin{aligned} J_i(\omega) &= \sum_x \omega_{x,i}^2 \lambda_{x,i}^2 \delta(\omega - \omega_x) \\ &= \frac{\lambda}{\omega_c} \omega e^{-\omega/\omega_c}, \end{aligned} \tag{43}$$

with $\omega_c = 100\, cm^{-1}$ and $\lambda = 30\, cm^{-1}$, which are typical energy scales for biomolecular chromophores. By applying second-order perturbation theory on H_{SB}, tracing over the degrees of freedom of B, and invoking the Markov and secular approximations, one can arrive at the Redfield equations [50]. The Redfield tensor has been computed as in reference [33]. Furthermore, phonon occupation numbers are evaluated at 273 K.